PLOS PATHOGENS

RESEARCH ARTICLE

Inducible CRISPR activation screen for interferon-stimulated genes identifies OAS1 as a SARS-CoV-2 restriction factor

Oded Danziger, Roosheel S. Patel, Emma J. DeGrace, Mikaela R. Rosen, Brad R. Rosenberg*

Department of Microbiology, Icahn School of Medicine at Mount Sinai, New York, New York, United States of America

* brad.rosenberg@mssm.edu

OPEN ACCESS

Citation: Danziger O, Patel RS, DeGrace EJ, Rosen MR, Rosenberg BR (2022) Inducible CRISPR activation screen for interferon-stimulated genes identifies OAS1 as a SARS-CoV-2 restriction factor. PLoS Pathog 18(4): e1010464. https://doi.org/10.1371/journal.ppat.1010464

Editor: Adrianus CM Boon, Washington University in Saint Louis School of Medicine, UNITED STATES

Received: January 7, 2022

Accepted: March 23, 2022

Published: April 14, 2022

Data Availability Statement: Sequence data files from inducible CRISPRa ISG screens are available from the NCBI Sequence Read Archive (SRA), accession number PRJNA777043. All other relevant data are within the manuscript and its supporting information files.

Funding: This work was supported in part by National Institutes of Health grants R01 AI151029 (B.R.R.) and U01 AI150748 (B.R.R.), and funds from the Icahn School of Medicine at Mount Sinai (B.R.R.). Research reported in this paper was also

Abstract

Interferons establish an antiviral state through the induction of hundreds of interferon-stimulated genes (ISGs). The mechanisms and viral specificities for most ISGs remain incompletely understood. To enable high-throughput interrogation of ISG antiviral functions in pooled genetic screens while mitigating potentially confounding effects of endogenous interferon and antiproliferative/proapoptotic ISG activities, we adapted a CRISPR-activation (CRISPRa) system for inducible ISG expression in isogenic cell lines with and without the capacity to respond to interferons. We used this platform to screen for ISGs that restrict SARS-CoV-2. Results included ISGs previously described to restrict SARS-CoV-2 and novel candidate antiviral factors. We validated a subset of these by complementary CRISPRa and cDNA expression experiments. OAS1, a top-ranked hit across multiple screens, exhibited strong antiviral effects against SARS-CoV-2, which required OAS1 catalytic activity. These studies demonstrate a high-throughput approach to assess antiviral functions within the ISG repertoire, exemplified by identification of multiple SARS-CoV-2 restriction factors.

Author summary

To counteract viral infection, interferon induces the expression of antiviral effectors collectively termed Interferon Stimulated Genes (ISGs). Different effector genes restrict different viruses through a variety of mechanisms. Identifying the particular ISGs that restrict specific viruses can uncover viral vulnerabilities and inform therapeutic strategies. Here, we developed a CRISPR-activation (CRISPRa) experimental strategy for screening hundreds of pooled ISGs for antiviral activity in parallel while accounting for the ability of some ISGs to inhibit cell cycle and to promote cell death. We applied this approach to detect ISGs that restrict SARS-CoV-2, the virus that causes COVID-19. In a series of controlled experiments, we identified multiple ISGs that counteract SARS-CoV-2 infection, and further validated a subset of these ISGs through focused CRISPRa and cDNA expression studies. Our results validate several previously identified ISGs, and identify multiple

supported by the Office of Research Infrastructure of the National Institutes of Health under award numbers S10OD018522 and S10OD026880. The content is solely the responsibility of the authors and does not necessarily represent the official views of the funders, including the National Institutes of Health. The funders had no role in study design, data collection and analysis, decision to publish, or preparation of the manuscript.

Competing interests: In compliance with PLOS Pathogens competing interests policy, the authors note that a provisional patent application has been filed that includes some aspects of the inducible CRISPR activation system described herein, with OD and BRR listed as inventors. All authors declare no other competing interests.

novel antiviral effectors with activity against SARS-CoV-2. Overall, our work demonstrates an experimental system for the controlled assessment of ISG antiviral activities, and expands the present understanding of innate antiviral defense against SARS-CoV-2.

Introduction

Interferons (IFN) act as key mediators of the host response to viral pathogens by establishing a general antiviral state through the coordinated induction of hundreds of interferon stimulated genes (ISGs) in infected and uninfected "bystander" cells [1]. ISGs encode functionally diverse gene products, including antiviral effectors that antagonize distinct steps of viral life cycles [2], but the antiviral mechanisms of most individual ISGs remain unknown. Studies that have systematically characterized the effects of single ISGs have demonstrated that a limited number of individual ISGs, primarily transcription factors and DNA/RNA sensors, can broadly restrict infection by multiple viruses upon overexpression in target cells [3–7]. Other individual ISGs have been found to restrict or even to enhance the replication of specific viruses. In addition to direct antiviral effectors, the ISG repertoire also includes genes that induce antiproliferative and/or proapoptotic programs in response to viral infection or DNA damage, thereby limiting viral spread and impeding oncogenesis [8–11].

A robust IFN response is critical for host defense against novel respiratory viruses to which immune memory from prior exposure has not been established [12]. As such, multiple lines of evidence have implicated IFN as a key component of the host response to Severe acute respiratory syndrome coronavirus 2 (SARS-CoV-2), the etiologic agent of COVID-19. Although IFN can effectively block SARS-CoV-2 infection *in vitro* [13–16], the activity of IFN in different physiological contexts is more complex. Characterizations of the IFN response to SARS-CoV-2 infection in a variety of model systems suggest that SARS-CoV-2 infection may not elicit robust IFN production and ISG expression, but can induce high levels of proinflammatory cytokines [17]. These findings are consistent with single cell RNA sequencing (scRNA-seq) immune profiling studies that have reported inflammatory gene signatures and less robust IFN/ISG expression in immune cells from individuals infected with COVID-19 as compared to individuals infected with Influenza [18]. However, transcriptomic analyses of bronchoalveolar lavage fluid (BALF) from COVID-19 patients detected a strong ISG signature along with proinflammatory cytokine gene expression in immune cells [19]. Dysregulation of the IFN response in SARS-CoV-2 infection can be driven by both direct viral antagonism of innate immune mechanisms, as well as by host characteristics such as age, genetics and other comorbidities [20]. Additionally, several studies have identified autoantibodies against IFN as a significant negative survival factor for severe COVID-19, further emphasizing the prominent role of IFN in SARS-CoV-2 pathogenesis and clearance [21–24]. Importantly, IFN-mediated effects may also be detrimental to COVID-19 outcomes. For example, disruption of the lung epithelium by type III IFN-dependent processes has been hypothesized to expose patients to secondary infections by opportunistic bacteria [25]. Taken together, while IFN and the downstream expression of ISGs can functionally restrict SARS-CoV-2, the site(s), cell types, amount, and timing of IFN production and response play critical roles in COVID-19 pathogenesis and outcomes.

The specific mechanisms by which IFN restricts SARS-CoV-2 have not been fully characterized. To date, of the hundreds of ISGs, only a handful have been found to restrict SARS-CoV-2 infection in different *in vitro* systems. Lymphocyte antigen 6 complex, locus-E (LY6E) was identified as a SARS-CoV-2 restriction factor in ISG ectopic cDNA expression screens

[26]. A transposon-mediated screen identified the MHC-II invariant chain CD74 as a block to SARS-CoV-2 entry [27]. In addition, overexpression of *BST2* (encoding Tetherin), an anti-HIV effector that prevents the release of nascent virions [28], has also been found to restrict SARS-CoV-2 by impeding virion release [29]. TRIM25, an interferon-induced E3 ubiquitin ligase that enhances antiviral responses downstream of RIG-I, has been shown to interact specifically with SARS-CoV-2 RNA and thereby reduce infection [30]. During preparation of this manuscript, two additional studies employing different expression systems and screening methodologies highlighted the prominent role of OAS1 in restricting SARS-CoV-2 [31,32].

Studies evaluating the antiviral potential of individual ISGs are often implemented through the ectopic expression of ISG cDNA libraries followed by viral challenge to screen for those ISGs that confer resistance [3,4,29,33,34]. While effective in identifying the antiviral potential of many ISGs, arrayed ISG cDNA screens are not without drawbacks including limited throughput, technically demanding cloning and validation of individual expression constructs, and high costs. Ectopic cDNA overexpression can be prone to artifactual expression patterns or functions [35,36]. In addition, cDNA expression screen libraries typically include only one isoform per gene, and therefore may overlook isoform-specific antiviral activities, as have been described for many ISGs [27,37–41].

CRISPR-activation (CRISPRa), in which guide RNA (gRNA)-directed endonuclease-deficient Cas9 along with transcriptional activators are targeted to a gene of interest (GOI) to induce expression, offers an alternative to cDNA ectopic expression screens. Advantages include easy to produce gRNA libraries, physiologically relevant expression levels, and multiplexing capabilities [42]. Gene transcription is initiated from endogenous promoters, and therefore has the potential to generate multiple isoforms for genes with alternative splicing programs. Studies in which genome-wide libraries of activating gRNAs uncovered important host factors in viral infection systems provide an important proof of concept to the characterization of ISGs using CRISPRa [43–45]. Importantly, two recent preprints report genome-wide CRISPRa screens for genes with antiviral potential against SARS-CoV-2 [46,47].

Here, we report an ISG-focused CRISPRa screen to identify ISGs that modulate SARS-CoV-2 infection in lung epithelial cells. To mitigate the potential antiproliferative and/or proapoptotic effects of certain ISGs that could impact their library representation, we engineered a Doxycycline (Dox)-inducible CRISPRa system that enables precise temporal control of ISG induction. Using a pooled screen strategy, we tested more than 400 ISGs for effects on SARS-CoV-2 infection in both wildtype cells and isogenic cells engineered to be insensitive to IFN. High ranking antiviral ISG hits included SARS-CoV-2 restriction factors previously identified in recent screens (*LY6E* [26], *CD74* [27], *TRIM25* [30] and *ERLIN1* [29]). We identified and validated previously undescribed antiviral roles for additional ISGs such as *CTSS* (Cathepsin S). In agreement with Wickenhagen *et al.* and Soveg *et al.*, [31,32] we also identified *OAS1* (2′-5′-oligoadenylate synthetase 1) as a SARS-CoV-2 restriction factor capable of inhibiting viral infection and the generation of progeny virus. Taken together, our findings demonstrate the utility of a novel inducible CRISPRa platform for antiviral genetic screens and identify multiple ISGs capable of restricting SARS-CoV-2.

Results

Inducible CRISPRa system in A549 cells

We developed an optimized platform for pooled, positive selection ISG screens by adapting the well-established SunTag CRISPRa technology [48], and engineering it into A549 lung adenocarcinoma cell lines, a widely employed model for respiratory virus infection [49–51]. First, we reasoned that the antiproliferative and/or proapoptotic properties of some ISGs [52] could

affect their relative representation in pooled libraries prior to infection experiments and/or independent of potential effects on virus susceptibility. To mitigate these effects, we reengineered the transcriptional transactivator component construct of the SunTag CRISPRa system to allow for Doxycycline (Dox)-inducible expression, and thereby Dox-inducible regulation of gRNA-targeted gene expression (Fig 1A). Next, we expected that IFN secretion in response to infection, with corresponding autocrine and paracrine induction of broad ISG expression throughout cultures, could interfere with assessments of individual CRISPRa-induced ISG effects within different cells in pooled screen experiments. Therefore, we transduced the modified SunTag components into A549$^{\Delta STAT1}$ cell lines [53] defective in their capacity to respond to IFN (A549$^{\Delta STAT1}$-SunTag), as well as the STAT1-competent A549 cell line (A549-SunTag, intact IFN response) from which they were derived. After selecting and expanding dual antibiotic-resistant single cell clones, we evaluated their capacity for Dox-inducible, gRNA-targeted gene expression. We transduced A549-SunTag and A549$^{\Delta STAT1}$-SunTag cell lines with lentiviral constructs expressing gRNAs targeting the promoter region of *MX1*, a well-characterized ISG that restricts multiple viruses [54,55], as well as with non-targeting gRNA (NTG) controls. Following puromycin selection of gRNA-transduced cells, cultures were treated with Dox for 48 hours, and *MX1* mRNA expression was assessed by quantitative RT-PCR (qRT-PCR). In both A549-SunTag and A549$^{\Delta STAT1}$-SunTag genotypes, Dox induced robust increases in *MX1* mRNA in cells expressing *MX1* gRNAs (Fig 1B), while Dox treatment of cells expressing NTG or non-transduced cells exhibited minimal changes in *MX1* gene expression. Comparison to cells pretreated with IFNα2b indicated that CRISPRa induced *MX1* mRNA expression to similar levels (Fig 1B). Interestingly, baseline levels of *MX1* mRNA exhibited higher Ct values in A549$^{\Delta STAT1}$ cells compared to their STAT1-competent A549 counterparts, resulting in greater fold change values for *MX1* expression upon Dox treatment (Fig 1B and 1C). This suggests that, even in the absence of exogenous IFN stimulation, some ISGs exhibit some level of constitutive STAT1-dependent transcription [56].

Next, we evaluated the functional antiviral capacity of an ISG in our CRISPRa cells. A549-SunTag and A549$^{\Delta STAT1}$-SunTag cells, transduced and selected to express *MX1* gRNA, were treated with Dox and infected with a GFP-encoding Indiana vesiculovirus (VSV-GFP [57]). Flow cytometry analysis, using GFP expression as a marker for productive infection, demonstrated a near-complete block of infection in Dox^{On} A549-SunTag cells with active *MX1* expression; Dox^{Off} cells and cells expressing an NTG were not protected (Fig 1D and 1E). While we also observed a protective effect in A549$^{\Delta STAT1}$-SunTag, a considerable fraction of cells remained susceptible to infection. These results indicate that Dox-inducible, CRISPRa-mediated ISG expression can effectively restrict viral infection. Furthermore, the restriction of VSV-GFP infection by MX1 is enhanced by additional, STAT1-dependent factors likely elicited by IFN production, further highlighting the utility of a STAT1-deficient screening platform for assessing the antiviral activity of individual ISGs. In sum, we established a functional, Dox-regulated CRISPRa system in isogenic cell lines with either intact or deficient IFN responses that effectively restricts viral infection upon induced expression of antiviral ISGs.

Inducible CRISPRa ISG screen for SARS-CoV-2 restriction factors

To identify ISGs that restrict SARS-CoV-2, we conducted pooled gene activation screens in our engineered CRISPRa A549-SunTag lines. Our general screening strategy was to evaluate the potential of hundreds of individual ISGs to confer resistance to the cytopathic effects (CPE) of SARS-CoV-2. We began by introducing ACE2 expression into A549-SunTag and A549$^{\Delta STAT1}$-SunTag cells to enable productive SARS-CoV-2 infection of our CRISPRa cells. Next, we conducted pilot experiments evaluating SARS-CoV-2 CPE for optimization of screen

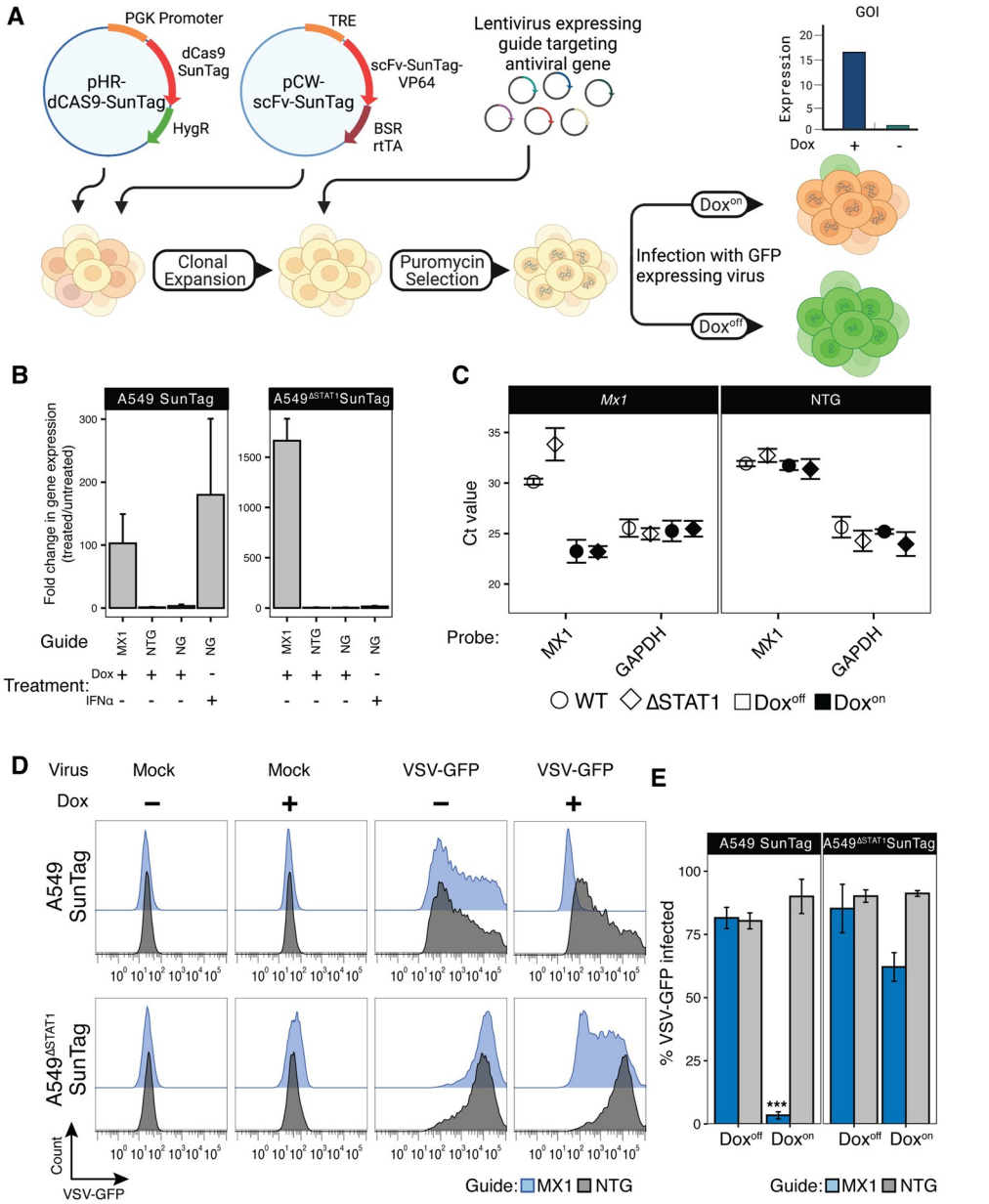

Fig 1. Inducible CRISPRa system demonstrates Dox-regulated, gRNA-specific gene expression and functional block of VSV-GFP infection in isogenic A549 and A549$^{\Delta STAT1}$ cell lines. **(A)** Schematic of the Dox-inducible CRISPRa system for assessing antiviral ISG activities. **(B)** qRT-PCR analysis for *MX1* mRNA in A549-SunTag and A549$^{\Delta STAT1}$-SunTag cells transduced with *MX1* gRNA, non-targeting gRNA (NTG), or in cells with no gRNA (NG), treated with Dox or IFN. Fold change gene expression in Dox^{on} cells relative to Dox^{off} cells calculated using the ΔΔCt method with normalization to *GAPDH*. **(C)** Mean qRT-PCR threshold cycle (Ct) values for *MX1* and *GAPDH* mRNA in A549-SunTag and A549$^{\Delta STAT1}$-SunTag cells transduced with *MX1* gRNA or NTG gRNA (NTG). Error bars indicate ± SD. **(D)** Representative flow cytometry histograms for GFP fluorescence in A549-SunTag and A549$^{\Delta STAT1}$-SunTag transduced with *MX1* gRNA (blue) or NTG (gray) gRNA and infected with VSV-GFP (M.O.I. = 1, 24hr). **(E)** Percent VSV-GFP-positive cells by flow cytometry quantified for n = 3 biological replicates. Bars represent mean ± SD of GFP positive cells across all replicates. Paired ratio Student's t-test, *** $p < 0.0005$.

https://doi.org/10.1371/journal.ppat.1010464.g001

conditions to balance the strength of selective pressure with its duration for robust detection of hits [58]. A549-SunTag ACE2 and A549$^{\Delta STAT1}$-SunTag ACE2 cells were transduced with expression constructs for gRNAs targeting *LY6E*, a known SARS-CoV-2 restriction factor

[26], or NTGs. Following Dox treatment, cultures were infected with SARS-CoV-2 at a range of multiplicities of infection (M.O.I.), plates were fixed every 24 hours, and cell viability was estimated by Methylene blue assay (S1A Fig). Dox^{On} cultures expressing *LY6E* gRNAs exhibited increased viability when infected with SARS-CoV-2. Moreover, A549-SunTag ACE2 cultures exhibited less CPE than $A549^{\Delta STAT1}$-SunTag ACE2 cultures, implicating additional STAT1-dependent antiviral factors. Based on these data, we approximated optimal infection conditions for ISG screens (M.O.I. = 3, harvest at 72 hours post-infection).

To construct an ISG gRNA library for screening, we merged lists of ISGs tested in previous studies [3,4] with a list of genes upregulated by IFNβ treatment in A549 cells [53] (log_2 fold-change >2, adjusted p value < 0.05). To focus on antiviral effectors, we excluded known transcription factors [59], several central Pattern Recognition Receptors (PRRs), and Human leukocyte antigen (HLA) genes (S1 Table contains the full list of ISGs in the library). For each ISG, we selected 3 gRNA sequences from the optimized Calabrese CRISPRa collection [60]. ISG gRNA sequences were supplemented with an additional 24 NTG controls, for a final list of 1,266 gRNAs targeting 414 ISGs (S2 Table).

Gene activation screens were conducted in both A549-SunTag ACE2 and $A549^{\Delta STAT1}$-SunTag ACE2 cells, in multiple independently transduced clones, across two independent experiments. A549-SunTag ACE2 and $A549^{\Delta STAT1}$-SunTag ACE2 cells were transduced with our ISG gRNA library (M.O.I. = 0.1), puromycin selected, and expanded. 48 hours prior to SARS-CoV-2 infection, appropriate cultures were treated with Dox to induce ISG expression (Fig 2A). All experiments included Dox^{Off} and Dox^{On} conditions, each of which included Mock or SARS-CoV-2 infection. At 72 hours post-infection, gRNA libraries were prepared from surviving cells and sequenced to assess gRNA relative enrichment/depletion. As we observed somewhat more CPE than expected in the first experiment, we slightly relaxed the selection pressure in the second experiment (additional wash for excess virus, details in *Materials and Methods*). All samples passed quality control metrics for multiple parameters as previously defined [61], exhibiting a high number of reads/sample and a high ratio of mapping between reads to the gRNA library (mean = 73%, SD = ± 5%) (S1B Fig). Mapped read counts were normalized within each genotype to allow for comparative analysis of gRNA enrichment/depletion (S1C Fig). To take advantage of our Dox-inducible system and replicated design for rigorous detection of ISG effects on SARS-CoV-2, we used MAGeCK-MLE [61,62] to test differential gRNA enrichment with a linear model including factors for Dox treatment (Off/On), SARS-CoV-2 infection status (Mock/Infected), Clone (independent gRNA library transduction 1/2), and Experiment (1/2, Full screen results: S3 Table). Importantly, this analysis strategy enabled assessment of ISG effects on SARS-CoV-2 in the context of potential antiproliferative/proapoptotic ISG effects that might independently alter gRNA abundance (assessed by Dox^{On} Mock *vs* Dox^{Off} Mock and corresponding interaction term in the model).

To identify ISGs with an effect on SARS-CoV-2 CPE in A549-SunTag ACE2 or $A549^{\Delta STAT1}$-SunTag ACE2 cells, we applied a stringent two-tiered set of filters for gRNAs differentially altered by SARS-CoV-2 infection. "Antiviral" and "proviral" (as determined by MAGeCK-MLE β-score [61] for Dox^{On} infected *vs*. Dox^{Off} infected coefficients) ISG hits were identified based on statistical significance for infection status (FDR < 0.1), while accounting for the effect of Dox treatment on gRNA abundance (linear model interaction FDR < 0.1). This strategy enabled robust identification of ISGs for which effects on SARS-CoV-2 infection were significantly stronger than their effects in mock infected cultures (e.g. due to antiproliferative, pro-apoptotic, or other effects). We detected 6 and 24 ISGs as "antiviral" (i.e. enriched by SARS-CoV-2 infection, Fig 2B and 2C) in A549-SunTag ACE2 and $A549^{\Delta STAT1}$-SunTag ACE2, respectively. Conversely, we detected 10 and 2 ISGs as "proviral" (i.e. depleted by SARS-CoV-2 infection, Fig 2B and 2C) in A549-SunTag ACE2 and $A549^{\Delta STAT1}$-SunTag

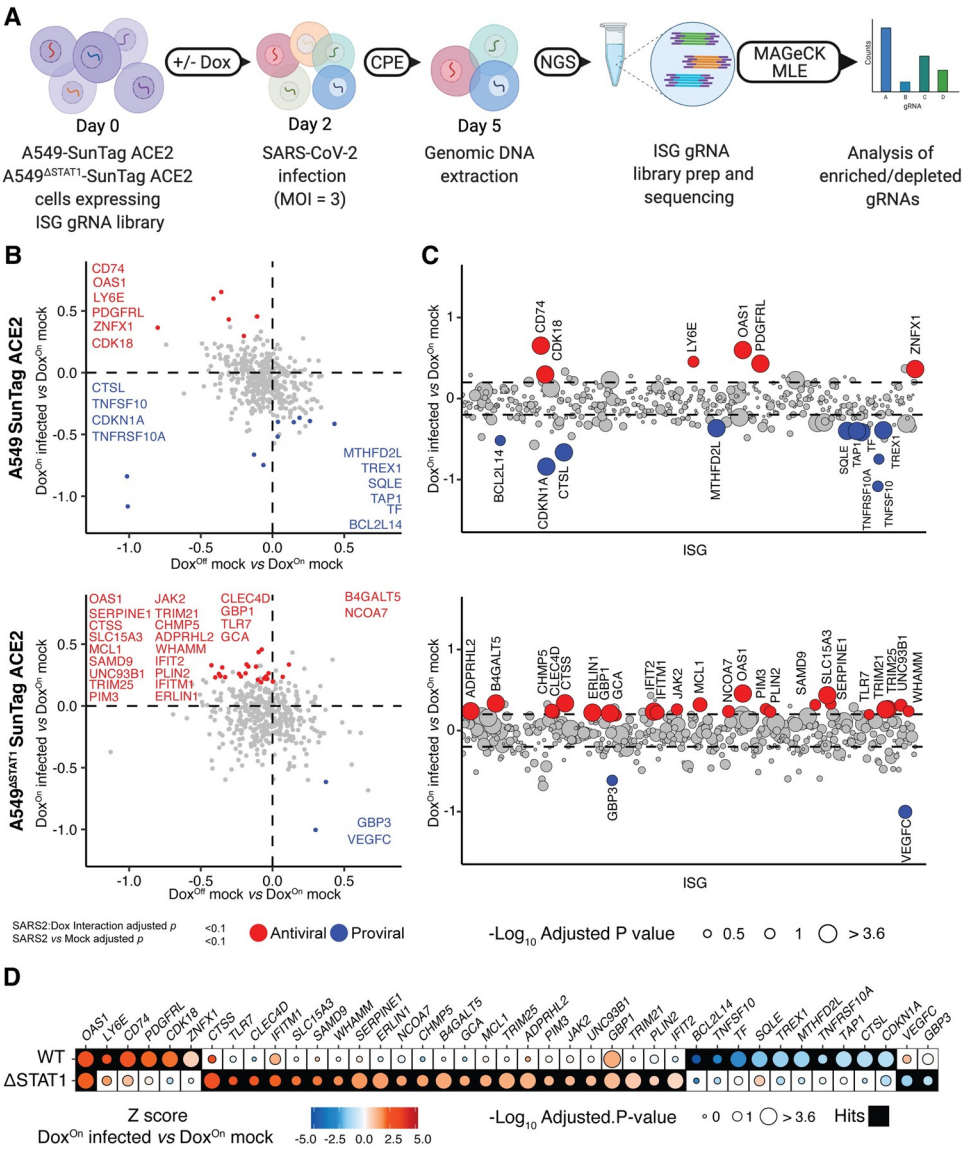

Fig 2. Inducible CRISPRa ISG screen for SARS-CoV-2 restriction factors. (A) Schematic of inducible CRISPRa ISG screens for SARS-CoV-2: Single cell clones of A549-SunTag ACE2 and A549$^{\Delta STAT1}$-SunTag ACE2 cells were transduced with a library of 1,266 gRNAs and infected with SARS-CoV-2 (M.O.I. = 3, 72 hours). After onset of SARS-CoV-2 CPE, genomic DNA was extracted from surviving cells, and enriched/depleted gRNAs were evaluated by high throughput sequencing followed by MAGecK MLE analysis. **(B)** MAGeCK-MLE analysis of SARS-CoV-2 ISG screens in A549-SunTag ACE2 and A549$^{\Delta STAT1}$-SunTag ACE2 cells. Plot depicts MAGeCK MLE β scores for Dox status coefficient (Dox^{Off} mock infected *vs* Dox^{On} mock infected, x-axis), and SARS-CoV-2 infection status coefficient (Dox^{On} SARS-CoV-2 infected *vs* Dox^{On} mock infected, y-axis). ISGs passing significance selection filters (SARS-CoV-2 infection status adjusted p value and SARS-CoV-2:Dox interaction adjusted p value < 0.1) are highlighted in red/blue for "antiviral"/"proviral" effects, respectively. SARS-CoV-2 restriction factors and antiproliferative genes are labeled with gene symbols. **(C)** MAGeCK-MLE analysis of SARS-CoV-2 ISG screens in A549-SunTag ACE2 and A549$^{\Delta STAT1}$-SunTag ACE2 cells, aligned by ISG. MAGeCK MLE β scores for SARS-CoV-2 infection status coefficient (Dox^{On} SARS-CoV-2 infected *vs* Dox^{On} mock infected) are plotted for each ISG (x-axis, alphabetical order); dots are sized according to significance of SARS-CoV-2:Dox interaction coefficient (-Log$_{10}$ adjusted p value) and highlighted in red/blue as in (B). Dashed line indicates ± 1 standard deviation of SARS-CoV-2 infection status coefficient β scores. **(D)** Comparison of candidate "antiviral"/"proviral" ISG hits passing significance filters in at least one (A549-SunTag ACE2 or A549$^{\Delta STAT1}$-SunTag ACE2) genotype. Dots are shaded by ISG Z-scores for SARS-CoV-2 infection status coefficient (Dox^{On} SARS-CoV-2 infected *vs* Dox^{On} mock infected), and sized according to the significance of SARS-CoV-2:Dox interaction coefficient (-Log$_{10}$ adjusted p value). Filled boxes indicate ISG passing significance filters for the indicated screen.

https://doi.org/10.1371/journal.ppat.1010464.g002

ACE2, respectively. Antiviral hits in at least one screen (i.e A549-SunTag ACE2 or A549$^{\Delta STAT1}$-SunTag ACE2) included *LY6E*, *CD74*, *TRIM25* and *IFITM1* (Fig 2B and 2C), each of which has been previously reported to restrict SARS-CoV-2 [26,27,30,63]. Proviral hits in at least one *STAT1* genotype included *CTSL* (encoding Cathepsin L), an entry factor for coronaviruses [64]. Additional proviral hits *CDKN1A* (p21) and *TNFRSF10A*, ISGs with antiproliferative and/or proapoptotic effects [65,66], were depleted upon Dox treatment independently of viral infection, and were further depleted by SARS-CoV-2 infection. This is in line with previous observations that coronaviruses require cell cycle inhibition for optimal replication [67]. Interestingly, when comparing ISG hits between A549-SunTag ACE2 and A549$^{\Delta STAT1}$-SunTag ACE2 screens (Fig 2D), we found only a single common antiviral hit across genotypes: *OAS1* (encoding 2′-5′-oligoadenylate synthetase 1). Not surprisingly, our results suggest that STAT1-dependent transcription, perhaps in response to endogenous IFN production in A549-SunTag ACE2 screens, modulates detection of CRISPRa-induced ISG effects on SARS-CoV-2. As illustrated in Fig 2D, many of our ISG hits were similarly selected in both *STAT1* genotypes (i.e. both antiviral or both proviral), but failed to clear significance thresholds in one of the screens. These discrepancies may be due to differences in relative enrichment (i.e. against all individual ISGs in the screen) of particular ISGs in IFN-responsive *versus* STAT1-deficient contexts. In sum, in conducting focused CRISPRa ISG screens for cell viability effects in A549 cells infected with SARS-CoV-2, we detected several previously known SARS-CoV-2 restriction factors as well as identified new candidate ISGs with putative anti-SARS-CoV-2 activities.

Comparison to other ISG-focused screens highlights common and unique antiviral hits

To date, two published studies report focused ISG screens for host factors with antiviral activity against SARS-CoV-2 [29,31]. Wickenhagen *et al.* and Martin-Sancho *et al.* both employ arrayed expression strategies coupled with flow cytometry or microscopy infection readouts, respectively. Together with our present study, which utilizes a pooled expression approach, ISG-focused screens have evaluated 637 distinct genes in the context of SARS-CoV-2 infection and identified multiple antiviral hits. Each study evaluated different sets of ISGs, due to different inclusion criteria in library construction and/or the availability of sequence-verified cDNA clones for arrayed experiments. Intersecting the ISG libraries of each study revealed a set of 224 ISGs assayed in all three screens, while highlighting that each study tested distinct collections of ISGs (S2A Fig). Somewhat surprisingly, in comparing ISGs designated "antiviral" by Wickenhagen *et al.*, Martin-Sancho *et al.* and our screens, we found only a single ISG (*LY6E*) common to all three studies (S2B Fig). A gene-level comparison of infection Z-scores, ranked from lowest (most inhibitory) to highest (least inhibitory) in each dataset, illustrated many similar trends in antiviral activities, but further exhibited the minimal overlap of significant hits across studies (S2C Fig). For example, IFITM3 was identified as a SARS-CoV-2 restriction factor by Martin-Sancho *et al.* [29], but did not clear significance thresholds in our screens or those reported by Wickenhagen *et al.* Other ISGs with evidence of restrictive activity against SARS-CoV-2, such as Z3CHAV1 (encoding ZAP) [68,69], were not reported as antiviral hits in any of the ISG screens. Such discrepancies may be attributable to differences in experimental systems (e.g. cell lines, ISG expression levels, and infection parameters). Additionally, differences from results presented here could be a result of screening methodology; unlike arrayed experiments, which evaluate the activity of individual ISGs, our pooled screening strategy evaluates relative enrichment/depletion of gRNAs, thereby highlighting the most inhibitory and enhancing ISGs in the tested set.

Validation of screen hits in targeted CRISPRa studies

To confirm hits identified in the pooled screens, we first conducted "single gene" validation experiments with the CRISPRa system for a subset of candidate antiviral ISGs. A549-SunTag ACE2 and A549$^{\Delta STAT1}$-SunTag ACE2 cells were transduced with expression constructs for gRNAs targeting one of eight antiviral ISG hits (*CD74*, *LY6E*, *OAS1*, *CTSS*, *TRIM25*, *ERLIN1*, *ADPRHL2*, *GBP1*) or with one of two NTGs, treated with Dox to induce gene expression, and infected with SARS-CoV-2. Compared to screening experiments (M.O.I. = 3), which were designed to select cells resistant to CPE in the context of extensive cell death, infection conditions in validation experiments were reduced slightly (M.O.I. = 2) to retain sufficient viable cells for downstream readouts. Dox-inducible, gRNA-specific CRISPRa-mediated expression for select genes (*CD74*, *CTSS* and *OAS1*) was confirmed in complementary qRT-PCR experiments (S3A and S3B Fig). We assessed the fraction of infected cells in Dox^{On} cultures (relative to fraction of infected cells in corresponding paired Dox^{Off} cultures, set to 100%) at 24 and 72 hours post-infection. At 24 hours, the fraction of SARS-CoV-2 infected cells (evaluated by flow cytometry for SARS-CoV-2 N protein) was significantly reduced in both A549-SunTag ACE2 and A549$^{\Delta STAT1}$-SunTag ACE2 cultures transduced with gRNAs targeting SARS-CoV-2 restriction factors *CD74* [27] and *LY6E* [26] (Fig 3A and 3B). SARS-CoV-2 infection was also significantly reduced by activation of *OAS1* expression in both A549-SunTag ACE2 and A549$^{\Delta STAT1}$-SunTag ACE2 cultures, while *TRIM25* expression demonstrated significant restriction only in A549-SunTag ACE2 cells (Fig 3A and 3B). Of note, TRIM25 enhances RIG-I signaling [70] and has been shown to interact with SARS-CoV-2 RNA [30], which may suggest that a consequent antiviral effect may require intact IFN signaling. Although some other hits exhibited consistent modest evidence of viral restriction (e.g. *CTSS*), no additional genes met statistical significance thresholds at the 24 hour time point.

Several additional hits were confirmed to be antiviral at 72 hours post infection. Once again, the fraction of SARS-CoV-2 infected cells (here assessed by high-throughput microscopy for SARS-CoV-2 N protein due to CPE/fragile cells) was significantly reduced in A549-SunTag ACE2 cultures with activated expression of *CD74*, *LY6E*, and *OAS1* (Fig 3C and 3D). We also observed significant reduction of infection in cultures expressing *CTSS* in both A549-SunTag ACE2 and A549$^{\Delta STAT1}$-SunTag ACE2 cultures, confirming its activity as a novel SARS-CoV-2 restriction factor. At this time point, *ERLIN1* expression also exhibited modest, yet significant, restriction of SARS-CoV-2 only in A549-SunTag ACE2 cells (Fig 3C and 3D). Ectopic expression of *ERLIN1*, a regulator of endoplasmic-reticulum-associated protein degradation (ERAD), was recently shown to restrict SARS-CoV-2 infection [29]. *ADPRHL2* and *GBP1*, additional ISGs identified as antiviral screen hits, did not reach statistical significance in CRISPRa validation experiments (S3C and S3D Fig). Taken together, these results confirm the antiviral effects of multiple ISG screen hits in our CRISPRa system, including *OAS1* and *CTSS*, against SARS-CoV-2.

Validation of screen hits by ectopic cDNA expression

To further validate antiviral hits confirmed in CRISPRa experiments with a complementary experimental system, we tested ectopically expressed ISG cDNAs for their ability to restrict SARS-CoV-2. A549 ACE2 and A549$^{\Delta STAT1}$ ACE2 cells (both without CRISPRa components) were transduced with Dox-inducible cDNA expression constructs for one of *CD74*, *LY6E*, *CTSS*, *TRIM25*, *ADPRHL2* or fLuc (Firefly luciferase, negative control; additional independent experiments for *OAS1* cDNAs are described in the following section). Comparison of protein expression patterns to corresponding CRISPRa cultures and assessments of Dox inducibility properties were carried out by immunoblot analysis of select screen hits (CD74 and CTSS,

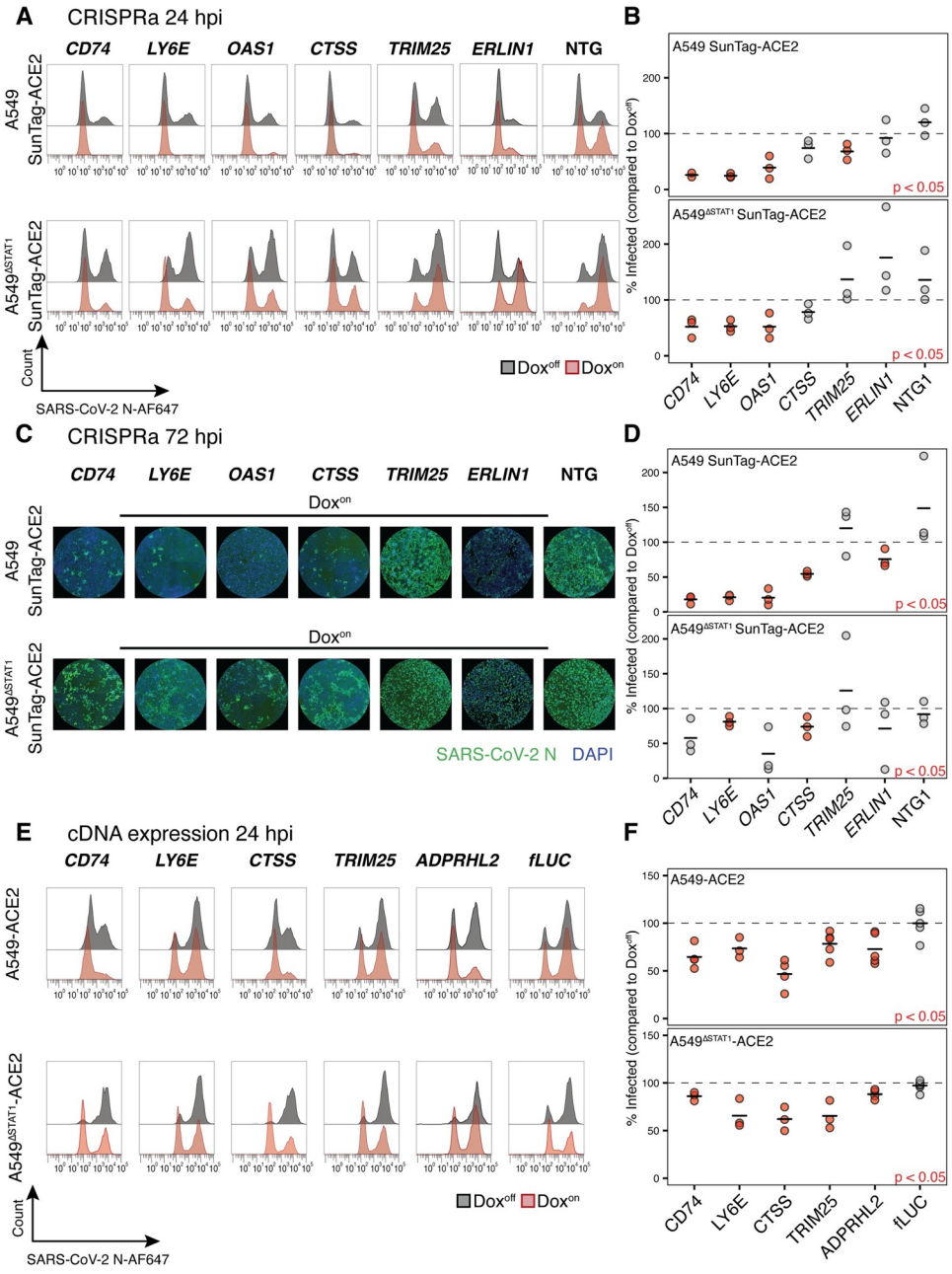

Fig 3. Validation of ISG screen hits in targeted CRISPRa and ectopic cDNA expression studies. (A) Representative flow cytometry histograms for SARS-CoV-2 N protein in A549-SunTag ACE2 and A549$^{\Delta STAT1}$-SunTag ACE2 transduced with indicated gRNAs, treated (red) or not treated (gray) with Dox, at 24 hours post-infection with SARS-CoV-2 (M.O.I. = 2). **(B)** Percent of infected (SARS-CoV-2 N protein positive) cells quantified across biological replicates (n = 3, n = 2 for *CD74* gRNA in A549-SunTag ACE2 cells) for experiments described in **(A).** Values denote percent of infected cells in Dox^{on} cultures relative to paired Dox^{off} cultures. Points represent individual biological replicates, black lines indicate mean values of biological replicates for each indicated ISG gRNA. Red points indicate statistical significance ($p < 0.05$) as determined by paired ratio Student's t-test. **(C)** Representative immunofluorescence images for SARS-CoV-2 N protein and DAPI in A549-SunTag ACE2 and A549$^{\Delta STAT1}$-SunTag ACE2 transduced with indicated gRNAs and treated with Dox, at 72 hours post-infection with SARS-CoV-2 (M.O.I. = 2). **(D)** Percent of infected (SARS-CoV-2 N protein positive) cells quantified across biological replicates (n = 3, n = 2 for ADPRHL2 gRNA in A549-SunTag ACE cells) for experiments described in (C). Values denote percent of infected cells in Dox^{on} cultures relative to paired Dox^{off} cultures. Points represent individual biological replicates, black lines indicate mean values of biological replicates for each indicated ISG gRNA. Statistical significance as in (B). **(E)** Representative flow cytometry histograms for SARS-CoV-2 N protein in A549 ACE2 and A549$^{\Delta STAT1}$ ACE2

transduced with expression constructs for indicated cDNAs (fLUC, firefly luciferase negative control), treated (red) or not treated (gray) with Dox, at 24 hours post-infection with SARS-CoV-2 (M.O.I. = 2). **(F)** Percent of infected (SARS-CoV-2 N protein positive) cells quantified across biological replicates ($n \geq 3$) for experiments in (E). Values denote percent of infected cells in Dox^{on} cultures relative to paired Dox^{off} cultures. Points represent individual biological replicates, black lines indicate mean values of biological replicates for each indicated ISG cDNA. Red points indicate statistical significance ($p < 0.05$) as determined by paired ratio Student's t-test.

https://doi.org/10.1371/journal.ppat.1010464.g003

S4A and S4B Fig). We observed Dox-inducible, robust protein expression of target genes from both cDNA and CRISPRa; no expression was detected in cultures transduced with firefly luciferase (fLUC) cDNA or NTG. For validation experiments, after antibiotic selection and expansion, cDNA expression was induced by Dox for 48 hours, after which cells were infected with SARS-CoV-2 (M.O.I. = 2). At 24 hours post-infection, the fraction of infected cells in Dox^{On} and Dox^{Off} conditions was assessed by flow cytometry for SARS-CoV-2 N protein. Dox-inducible cDNA expression of *CD74*, *LY6E*, *CTSS* and *TRIM25* recapitulated similar patterns of SARS-CoV-2 restriction (Fig 3E and 3F) observed in the CRISPRa system (Fig 3A–3D). In addition, *ADPRHL2*, ADP-ribose glycohydrolase, which has not been previously described as an antiviral effector, also significantly restricted SARS-CoV-2 in cDNA expression experiments (Fig 3E and 3F). Interestingly, the apparent antiviral effect conferred by cDNA expression of CD74 was weaker than that observed in corresponding CRISPRa gRNA-directed expression experiments (Fig 3E, compared to Fig 3A). Of note, the anti-SARS-CoV-2 effects of CD74 have been ascribed to the p41 isoform [27], while the "canonical" isoform p45 (Uniprot identifier P04233-1) was tested in our cDNA experiments. Interestingly, in immunoblot analysis (S4A Fig), CRISPRa induction of CD74 from its endogenous promoter in SunTag cells resulted in predominant expression of the potent antiviral p41 isoform. However, CD74 expression from cDNA resulted in only a faint band at the expected molecular size of 45kDa but a much stronger band at 37kDa, consistent with post-translational proteolytic cleavage known to regulate the localization and activity of CD74 [71]. The soluble form of CD74 (apparent as an immunoreactive band at 25kDa [72]), was also observed in both cDNA and CRISPRa expression systems. These discrepancies likely explain the modest restriction of SARS-CoV-2 by CD74 in cDNA expression experiments as compared to CRISPRa experiments, and further highlight the potential of CRISPRa in revealing potential isoform-specific ISG antiviral effects that could be overlooked in cDNA expression studies.

Characterization of OAS1 as a potent SARS-CoV-2 restriction factor

OAS1, identified as a SARS-CoV-2 restriction factor in several recent reports [31,32], was detected as an antiviral ISG hit in both A549-SunTag and $A549^{\Delta STAT1}$-SunTag screens (Fig 2) and validated in targeted CRISPRa experiments at both time points tested (Fig 3). The oligoadenylate synthetase (OAS) family of ISGs are key enzymes involved in antiviral defense [1]. Upon sensing cytosolic dsRNA, OAS proteins are activated to catalyze the formation of 2′-5′-linked oligoadenylate (2′-5′A), which in turn activates latent ribonuclease L (RNaseL). Active RNaseL directly combats diverse viruses by degrading viral genomes, and indirectly by degrading cellular RNA and tRNA [73]. In humans, three members of the OAS family (OAS1, OAS2, OAS3) are capable of synthesizing 2′-5′A, and differ by size and sensitivity to dsRNA. An additional family member, OASL, is deficient in 2′-5′A catalysis but can sense dsRNA and thereby enhance RIG-I signaling [74,75]. While we detected *OAS1* as a highly ranked hit in both A549-SunTag ACE2 and $A549^{\Delta STAT1}$-SunTag ACE2 screens, other OAS family members were not found to confer antiviral or proviral effects (Fig 4A).

Given its apparent potency in both IFN-responsive and non-responsive contexts, we focused additional studies on characterizing the antiviral activities of OAS1 on SARS-CoV-2

infection. Extending the single gene CRISPRa experimental design described above (Fig 3A–3D), we assessed the effects of gRNA-activated *OAS1* expression on cell viability during SARS-CoV-2 infection. Consistent with results from our positive selection cell survival screens, Dox induction of gRNA-mediated *OAS1* expression conferred a dramatic improvement in cell survival assessed at 72 hours post-infection in both A549-SunTag ACE2 and A549$^{\Delta STAT1}$-SunTag ACE2 cultures; Dox^{Off} cultures and cultures transduced with NTG were readily eliminated by infection (Fig 4B). In addition to protective effects on cell viability, we also tested the direct impact of *OAS1* expression on the propagation of SARS-CoV-2. To minimize the effects of endogenous IFN production on viral replication, we infected Dox^{Off} and Dox^{On} A549$^{\Delta STAT1}$ SunTag ACE2 cells expressing *OAS1* or NTG gRNAs with a low inoculum of SARS-CoV-2 (M.O.I = 0.05), and quantified viral titers by plaque assay over time. Activation of *OAS1* expression resulted in a significant decrease in the production of viral progeny, indicating that OAS1 activity functionally restricts SARS-CoV-2 infection (Fig 4C).

OAS1 isoforms have been shown to differ in their antiviral activities [38]. To evaluate potential isoform-specific effects of OAS1 on SARS-CoV-2 restriction, we transduced A549 ACE2 and A549$^{\Delta STAT1}$ ACE2 cells with Dox-inducible expression constructs for cDNAs encoding OAS1 canonical isoform p46 (OAS1p46, Uniprot identifier P00973-1) and a shorter OAS1 isoform (OAS1p42, Uniprot identifier P00973-2) that was recently suggested to be the highest expressed isoform of OAS1 in A549 cells [38]. To test the requirement of OAS1 catalytic activity for restricting SARS-CoV-2, we also transduced an expression construct for a catalytically inactive OAS1p46 in which amino acids 331, 332 and 333 are replaced with Alanine (OAS1p46$^{C331A/F332A/K333A}$) [76]. We also included constructs for OAS2, OAS3 and OASL cDNAs. Following antibiotic selection and expansion, cDNA expression was induced with Dox and validated by immunoblotting (Fig 4D). To assay for antiviral activity, cultures were infected with SARS-CoV-2 (M.O.I. = 2) and infection was assessed by flow cytometry (SARS-CoV-2 N protein) at 24 hours post infection (Fig 4E and 4F). As expected, Dox induction of OAS1p46 expression significantly reduced the fraction of infected cells in both A549 ACE2 and A549$^{\Delta STAT1}$ ACE2 cells. The p42 isoform of OAS1 exhibited similar restriction of infection. Inactivation of OAS1 catalytic activity completely ablated its antiviral effects, suggesting that the mechanism of *OAS1*-mediated SARS-CoV-2 restriction acts through downstream RNaseL activation. Interestingly, while expression of OAS3 exhibited some restriction of SARS-CoV-2 (significant only in A549 ACE2 cells), other OAS family members did not restrict SARS-CoV-2 infection (OAS2), or may have promoted SARS-CoV-2 infection (OASL, only in A549$^{\Delta STAT1}$ ACE2 cells).

Inducible CRISPRa ISG screen highlights ISGs with antiproliferative/proapoptotic effects

In addition to identification of potential antiviral genes, our experimental design enables indirect assessment of potential ISG effects on cell viability and proliferation outside the context of viral infection. To identify such ISGs, we evaluated significant enrichment/depletion according to their Dox status (Dox^{Off} mock infected *vs* Dox^{On} mock infected, adjusted p value < 0.1, S5A Fig). Most significant hits were depleted by Dox treatment (i.e. negatively selected upon expression). Indeed, gRNAs with significantly reduced representation in Dox^{on} conditions included target genes for apoptotic signaling (*TNFRSF10A*, *TNFAIP3*) and cell cycle negative regulation (*CDKN1A*). The small number of enriched gRNAs (i.e. positively selected upon expression) included Transferrin (*TF*) and Growth differentiation factor 15 (*GDF15*), both of which have been previously described to promote cell proliferation in A549 cells [77,78]. Negatively selected hits common to both A549-SunTag and A549$^{\Delta STAT1}$-SunTag screens included

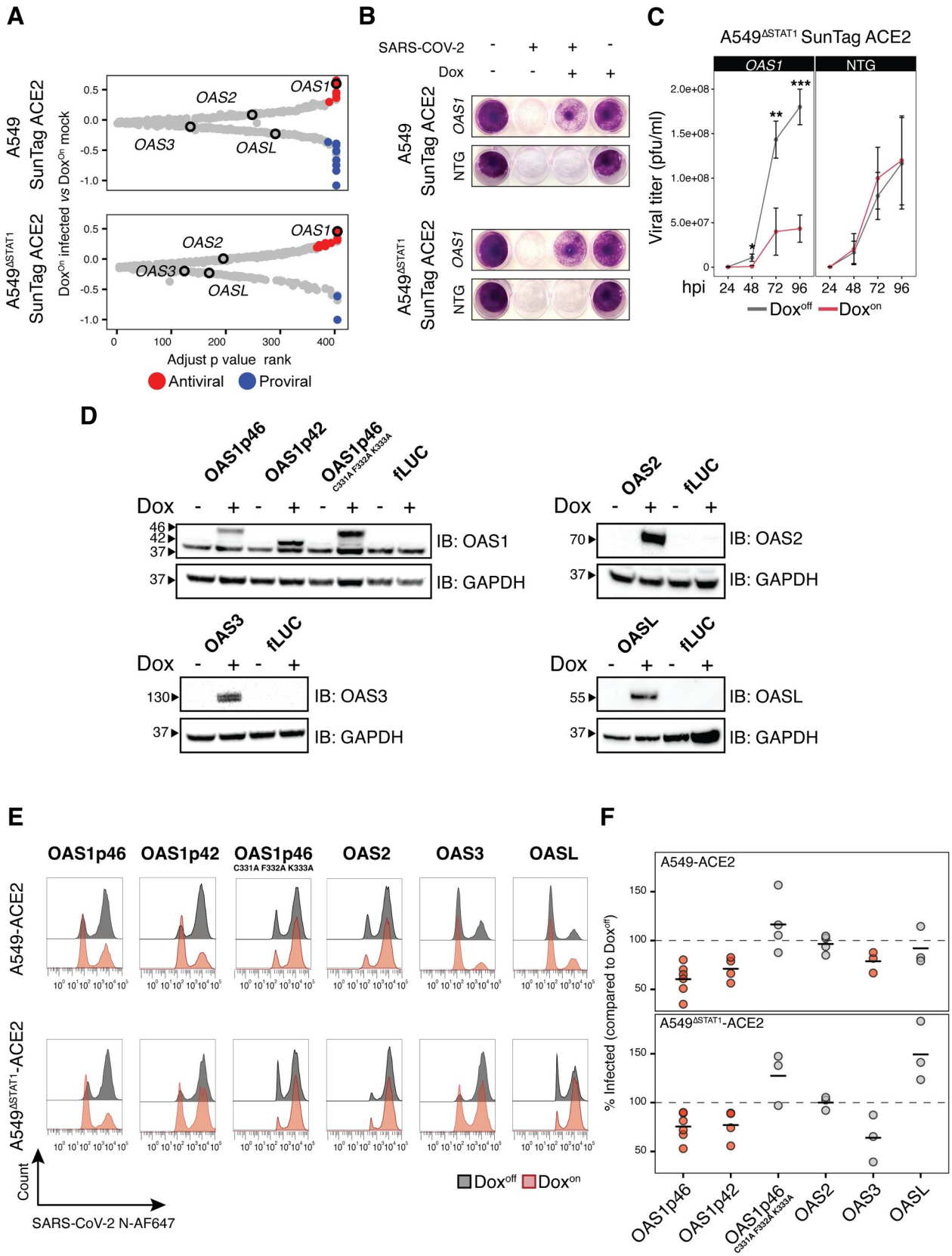
A
A549 SunTag ACE2
A549ΔSTAT1 SunTag ACE2
DoxOn infected vs DoxOn mock
OAS1
OAS2
OAS3
OASL
Adjust p value rank
Antiviral
Proviral
B
SARS-COV-2
Dox
A549 SunTag ACE2
A549ΔSTAT1 SunTag ACE2
OAS1
NTG
C
A549ΔSTAT1 SunTag ACE2
OAS1
NTG
Viral titer (pfu/ml)
hpi
Doxoff
Doxon
D
OAS1p46
OAS1p42
OAS1p46 C331A F332A K333A
fLUC
OAS2
OAS3
OASL
IB: OAS1
IB: OAS2
IB: OAS3
IB: OASL
IB: GAPDH
E
A549-ACE2
A549ΔSTAT1-ACE2
Count
SARS-CoV-2 N-AF647
Doxoff
Doxon
F
A549-ACE2
A549ΔSTAT1-ACE2
% Infected (compared to Doxoff)

Fig 4. OAS1 is a potent SARS-CoV-2 restriction factor. (A) OAS family genes in inducible CRISPRa ISG screen results. For A549-SunTag ACE2 and A549$^{\Delta STAT1}$-SunTag ACE2 screens, ISGs were ranked by SARS-CoV-2:Dox interaction adjusted p value (x axis). β scores for SARS-CoV-2 infection status coefficient (Dox^{On} SARS-CoV-2 infected *vs* Dox^{On} mock infected) are plotted on the y axis, with points passing significance filters highlighted in red/blue for "antiviral"/"proviral" effects, respectively. OAS family members are labeled as indicated. **(B)** Images of A549-SunTag ACE2 and A549$^{\Delta STAT1}$-SunTag ACE2 cultures transduced with *OAS1* gRNA or NTG, treated/not treated with Dox and infected as indicated with SARS-CoV-2 (M.O.I. = 2, 72 hours infection). Cultures were fixed and stained with Crystal violet to visualize cell viability. **(C)** SARS-CoV-2 growth curves measured by plaque assay. A549$^{\Delta STAT1}$-SunTag ACE2 cells expressing *OAS1* gRNA or NTG gRNA were infected with SARS-CoV-2 (M.O.I. = 0.1) and culture media was collected at indicated time points (x-axis, hours post infection, hpi). Titer was determined by plaque assay on Vero-E6 cells. Statistical significance at each timepoint determined by two-sided Student's t-test, *** $p < 0.0005$, ** $p < 0.005$, * $p < 0.05$. **(D)** Immunoblot analysis of OAS1 isoforms, OAS1p46 catalytic inactive mutant, OAS2, OAS3 and OASL. Indicated genes were expressed from lentivirus vectors and gene expression was induced by Dox treatment for 48 hours prior to immunoblotting with indicated antibodies. fLUC-expressing vector was used as a negative control. **(E)** Representative flow cytometry histograms for SARS-CoV-2 N protein in A549 ACE2 and A549$^{\Delta STAT1}$ ACE2 transduced with expression constructs for indicated OAS family member cDNAs, treated (red) or not treated (gray) with Dox, at 24 hours post-infection with SARS-CoV-2 (M.O.I. = 2). **(F)** Percent of infected (SARS-CoV-2 N protein positive) cells quantified across biological replicates for experiments described in **(E)**. Values denote percent of infected cells in Dox^{on} cultures relative to paired Dox^{off} cultures. Points represent individual biological replicates, black lines indicate mean values of biological replicates for each indicated cDNA. Red points indicate statistical significance ($p < 0.05$) as determined by paired ratio Student's t-test.

https://doi.org/10.1371/journal.ppat.1010464.g004

CDKN1A, *TNFRSF10A* and *APOBEC3A*, all previously implicated in reducing proliferation [66,79,80], and *RNF213*, *MT1H*, *UBE2L6*, *JAK2* and *PXK*, without established roles in cell cycle and/or death pathways (S5B Fig). These results support potential functions for many ISGs, including many with established antiviral activities, in IFN effects on cell viability and proliferation.

Discussion

Here, we report a CRISPRa strategy for pooled screens of IFN-induced antiviral effectors, and employed this approach to identify ISGs that restrict SARS-CoV-2 cytopathogenicity. Screen results included previously described SARS-CoV-2 restriction factors, as well as multiple additional candidate ISGs with antiviral activity against SARS-CoV-2. Focused CRISPRa and cDNA validation experiments for a subset of these hits confirmed the protective effects of SARS-CoV-2 restriction factors, including *CTSS* and *OAS1*.

CRISPRa optimized for pooled antiviral ISG screens

CRISPRa strategies have recently been applied to identify genes that regulate viral infection. In a pooled CRISPRa screen, Heaton *et al.* identified host restriction factors for Influenza A Virus [43]. Using a similar genome-wide gRNA library in a different cell line, Dukhovny *et al.* detected antiviral effectors with activity against Zika Virus [44]. Recent preprints also reported genome-wide CRISPRa screens for SARS-CoV-2 [46,47]. While these examples demonstrate the utility of pooled CRISPRa screens for identifying viral restriction factors genome-wide, we aimed to establish a CRISPRa system optimized for efficiently evaluating ISG activities against respiratory viruses. First, we addressed the potentially confounding effects of endogenous IFN produced by infected cells by expressing the SunTag components in A549$^{\Delta STAT1}$ cells, which are deficient in their capacity to respond to IFN. Indeed, our SARS-CoV-2 CRISPRa ISG screens in A549 and A549$^{\Delta STAT1}$ cells returned almost completely distinct hit lists of candidate antiviral factors; while many ISGs demonstrated similar antiviral trends in both cell lines, only *OAS1* cleared selection thresholds in both systems. The expression of multiple ISGs can confer additive effects to viral restriction [3], which may explain this pattern of results.

Some ISGs suppress cell proliferation or promote apoptosis [1]. These molecular programs may limit viral spread and maintain genome integrity upon detecting nucleic acid damage. Prominent ISGs known to regulate the cell cycle and/or promote cell death include *CDKN1A* (p21) [79], *IFI27* [81], *XAF1* [82], and members of the oligoadenylate synthetase family of genes [83]. Assessing potential antiviral activities of such genes presents technical challenges,

particularly in pooled screen settings in which gene expression alone (and corresponding effects on cell proliferation and/or cell death) is likely to impact relative enrichment/depletion independently of viral infection. Several examples of regulatable CRISPRa systems have been recently described [84–86]. Our implementation of Dox-inducible SunTag CRISPRa gene expression enables transduction and expansion of cultures with gRNAs targeting antiproliferative/proapoptotic ISGs with minimal deleterious effects, as gene expression is only induced shortly before viral infection. Moreover, in comparing Dox^{On} and Dox^{Off} cultures in the absence of viral infection, we are able to assess the antiproliferative/proapoptotic effects of each ISG. Indeed, not only did our results include multiple known cell cycle regulators depleted after only 48 hours after Dox induction, but they also included genes (*CDKN1A*, *TNFRSF10A* and *OAS1*) with demonstrable effects on *both* virus-independent library enrichment/depletion *and* susceptibility to SARS-CoV-2. While the antiproliferative and proapoptotic effects of IFN are well established [52], a systematic analysis of the ISGs that mediate these effects remains to be conducted. The initial results and experimental framework described here could be further extended to a comprehensive appraisal of ISG effects on cell cycle and apoptosis. As many cancers exhibit dysregulated ISG expression, such analyses have the potential to inform a variety of therapeutic strategies, particularly oncolytic virus development.

Cathepsin S restricts SARS-CoV-2

Coronaviruses can enter cells via two different routes: from the cell membrane or from the endosomal compartment. The route of entry is determined in part by the presence of cellular proteases required for spike protein processing [87]. SARS-CoV-2 entry from the cell surface requires *TMPRSS2*, while endosomal entry is mediated by cathepsins that process the spike protein [87]. Cathepsins are cellular proteases that have been implicated in the entry processes of multiple viruses by activating viral glycoproteins to trigger viral fusion at the endosomal membrane [77]. Our screens found that expression of Cathepsin L (*CTSL*), an entry factor for coronaviruses [64], sensitizes cells to SARS-CoV-2 infection. Intriguingly, Cathepsin S (*CTSS*), an ISG in A549 cells [53], was identified and validated in our experiments to confer a survival benefit to cells challenged with SARS-CoV-2. Of note, A549 cells lack expression of *TMPRSS2* [88], making cathepsin glycoprotein processing and endosomal entry likely pathways in viral infection. The apparently opposing effects of *CTSL* and *CTSS* on SARS-CoV-2 infection are surprising and the mechanistic basis for this difference is unclear. *CTSS* and *CTSL* have been shown to bind and cleave different polypeptide motifs [89], raising the possibility that cleavage by *CTSS* results in suboptimal spike cleavage products that are dysfunctional for viral entry. Alternatively, *CTSS* may interfere indirectly with spike processing by other cathepsins such as *CTSL*. Of note, we found that CTSS maintains its restrictive function in $A549^{\Delta STAT1}$ cells, indicating that its activity against SARS-CoV-2 does not require IFN-induced factors such as *CD74*, which inhibits SARS-CoV-2 by blocking cathepsin-mediated entry [27].

OAS1 is a potent SARS-CoV-2 restriction factor

Oligoadenylate synthetase family members are broadly acting ISGs important for innate antiviral defense against multiple viruses [74]. RNaseL, the downstream effector of OAS1-3, degrades cellular and viral RNA upon activation and thereby limits viral propagation. RNaseL activity has been directly implicated in host defense against different coronaviruses [90,91], most recently against SARS-CoV-2 [92]. The OAS/RNaseL pathway is antagonized by MERS-CoV, which blocks RNaseL activation by degrading 2′-5′A species generated by OAS proteins [90]. Our screens identified OAS1 as a SARS-CoV-2 restriction factor in both A549-SunTag ACE2 and $A549^{\Delta STAT1}$-SunTag ACE2 cells. Our experiments further demonstrated that OAS1

catalytic activity is necessary for its effects on SARS-CoV-2. This observation suggests that SARS-CoV-2 may not directly antagonize the generation of 2′-5′A like MERS-CoV, and therefore remains susceptible to RNaseL effector functions [92].

A growing body of genetic, epidemiological, and clinical data support an important role for OAS1 in both SARS-CoV and SARS-CoV-2 host defense. *OAS1* genetic variants were linked to infection and excessive morbidity in the SARS-CoV outbreak [93,94]. More recently, genome-wide association studies (GWAS) have associated single nucleotide polymorphisms (SNPs) in *OAS* loci with COVID-19 mortality [95]. Clinical studies have shown that elevated levels of plasma OAS1 are associated with reduced COVID-19 hospitalization and mortality; these effects are amplified by an OAS1 isoform of Neanderthal origins [96]. While this manuscript was under preparation, two other studies identified OAS1 as a SARS-CoV-2 antiviral gene [31,32]. Wickenhagen, *et al*. and Soveg, *et al*. described an association between a prenylated isoform of OAS1 (p46) and COVID-19 outcomes, further underscoring the importance of OAS1 in SARS-CoV-2 pathogenesis. Both studies demonstrated that prenylated OAS1 is targeted to the endomembranous sites of SARS-CoV-2 replication. They both observed significantly more potent viral restriction by the OAS1p46 isoform than the OAS1p42 isoform, which lacks the CAAX box motif prenylation signal. Interestingly, although A549 cells are capable of expressing only the OAS1p42 isoform [31,38], we found OAS1 (expressed from its endogenous promoter via CRISPRa) as a top ranked hit in our screens. Furthermore, we observed SARS-CoV-2 restriction by both OAS1p42 (CRISPRa and cDNA) and OAS1p46 (cDNA) in follow up validation experiments. Wickenhagen, *et al*. did not detect antiviral activity for OAS1p42 in A549 cells expressing ACE2 and TMPRSS2, while Soveg, *et al*. observed viral restriction by OAS1p42 that was further enhanced by the prenylated OAS1p46 isoform in 293T cells. Our observation of antiviral activity for both OAS1p42 and OAS1p46 could be a consequence of the assays used, infection conditions, timepoints tested and/or differences in expression levels. It could also be possible that different SARS-CoV-2 lineages are differentially susceptible to OAS1 isoforms (infections in Wickenhagen, *et al*. were conducted with CVR-GLA-1, infections in Soveg, *et al*. and the present study were conducted with USA-WA1/2020).

In addition to apparent differences in isoform activity, given the potent effects of OAS1 in our experiments, we were surprised that it had not been detected in several other recently published genome-wide and ISG-focused screens [29,46,47,97,98]. This could be due to the distinct features of the experimental systems used, such as low M.O.I. infections of IFN-competent cell lines, in which potential paracrine signaling may obscure certain ISG effects. This possibility is generally supported by the relatively few ISGs detected in pooled activation screens [43,44,46,47], which would otherwise be predicted to be enriched due to their direct antiviral effects. Moreover, as *OAS1* has been characterized as proapoptotic [99], our inducible system and multifactorial analysis strategy may have been particularly capable to robustly detect its effects.

CRISPRa identification of ISGs that enhance SARS-CoV-2 cytopathogenicity

While our screens were primarily focused on identifying SARS-CoV-2 antiviral factors based on the enrichment of ISG gRNAs in cells protected from virus-mediated CPE, our experimental design enabled parallel identification of ISGs that sensitize cells to CPE based on relative depletion of gRNAs in infected cultures. We identified 12 factors that enhanced SARS-CoV-2 CPE, of which 6 have been previously identified as potential direct interactors with SARS-CoV-2 proteins (CTSL, SQLE, TAP1, TF, TNFRSF10A and TREX1) [100–104]. Of note,

several CPE-enhancing ISGs encode pro-apoptotic proteins (TNFRSF10A, BCL2L14 and TNFSF10). Our multifactorial analysis model suggested that gRNAs targeting these pro-apoptotic factors were additionally depleted beyond levels measured in mock-infected cultures, indicating that viral infection increased their effects. This is consistent with previous studies demonstrating the activation of programmed cell death by different coronavirus proteins [105,106]. Interestingly, both CTSL (a known coronavirus host factor) and TF (Transferrin) were identified as SARS-CoV-2 cellular host factors in recently published CRISPR-Cas9 gene disruption screens [107–109]. Taken together, these results further highlight the potential of inducible CRISPRa as a tool for simultaneous identification of antiviral restriction factors and cellular host factors that support viral processes.

Materials and methods

Cell lines and VSV-GFP

All cell lines used in this study were maintained in Dulbecco's Modified Eagle Medium (DMEM, Corning #10-017-CV) supplemented with 10% fetal-bovine serum (FBS) and 1% Penicillin Streptomycin (PSN, Fisher scientific #15-140-122), and routinely cultured at 37˚ C with 5% CO_2. Vero-E6 cells (ATCC, CRL-1586) were used for propagation of SARS-COV-2 and for plaque-assays. Lenti-X 293T cells (Takara #632180) were used for lentivirus packaging. A549 and A549$^{\Delta STAT1}$ [53], a kind gift from Dr. Meike Dittmann (NYU Langone School of Medicine), were used for generation of CRISPRa cell lines and for infection studies. A549 and derived cell lines (ACE2-expressing cell lines with or without CRISPRa expression and ΔSTAT1 counterparts) were validated by short tandem repeat (STR) analysis (all confirmed 100% match to A549, CVCL_0023). All cell lines were routinely tested (Boca Scientific #50-168-5641) negative for Mycoplasma contamination. Recombinant-Indiana vesiculovirus expressing GFP (VSV-GFP) was a gift from Dr. Dusan Bogunovic (Icahn School of Medicine at Mount Sinai). Propagation and infections were conducted as previously described [55].

Reagents and chemicals

For Dox treatments to induce gene expression (both CRISPRa cell lines and cDNA ORF expression constructs), cultures were incubated in DMEM 10% FBS supplemented with 5μg/ml Doxycycline (Sigma # 50-165-6938) for 48 hours prior to infection or culture harvest as indicated for each experiment. Infections (VSV-GFP, SARS-CoV-2) were performed for 1 hour at 37˚C in the absence of Dox, which was re-added (1μg/ml) upon removal of the virus inoculum. For IFN experiments, cultures were treated with 200U of recombinant human IFNα2b (PBL Assay Science # 11105–1) for 3 hours prior to culture harvest.

Propagation and titration of SARS-COV-2

SARS-COV-2 (isolate USA-WA1/2020, BEI resource NR-52281) stocks were grown by inoculating confluent T175 flasks of Vero-E6 cells with SARS-COV-2 isolate (passage 2). Infected cultures were maintained in reduced-serum DMEM (2% FBS) for 3 days, after which medium was collected and filtered by centrifugation (8000 x g, 15 minutes) using an Amicon Ultra-15 filter unit with a 100KDa cutoff filter (Millipore # UFC910024). Concentrated virus stocks in reduced-serum DMEM (2% FBS) supplemented with 50mM HEPES buffer (Gibco #15630080) were stored at -80˚C.

To determine the number of infectious units in each viral stock (IU/ml), target cell lines (A549-ACE2 or A549-SunTag-ACE2) were plated in duplicate in 24 well plates, and were infected with 2-fold serial dilution series of SARS-CoV-2 stocks at 37˚C for 1 hour, after which

virus was removed and replaced with DMEM supplemented with 10% FBS. At 24 hours post-infection, cultures were harvested and fixed by incubating in 4% Paraformaldehyde (Alfa Aesar #AA433689M) in PBS for 24 hours. The fraction of infected cells was determined by flow cytometry for SARS-CoV-2 N protein (details below). The percentage of infected cells was used to determine the IU/ml values for each viral stock by using the formula:

$$\frac{Dilution\ factor \times initial\ number\ of\ cells\ in\ well \times fraction\ of\ infected\ cells}{infection\ volume} = IU/ml$$

All SARS-CoV-2 propagations and experiments were performed in a biosafety level 3 facility in compliance with institutional protocols and federal guidelines.

Generation of lentiviruses and viral transduction

To generate lentiviruses for gRNA or cDNA expression, a mix of 2.5μg of the desired transfer vector, 2μg psPAX2 and 0.8μg of pMD2.G (a gift from Didier Trono, Addgene #12260 and #12259, respectively), 14μl Lipofectamine 3000 (ThermoFisher scientific #L3000001) and 20μl of P3000 reagent, was prepared in 250μl of OptiMEM (Gibco #11058021). This transfection mix was added to $1.5x10^6$ Lenti-X 293T cells (Takara Bio #632180, plated in 6 well plates 18 hours prior to transfection) in 1 ml of 10% FBS DMEM for 8 hours after which transfection media was removed and replaced with 2ml of 10% FBS DMEM. 3 days post-transfection lentivirus supernatants were collected and centrifuged at 800g for 5 minutes to pellet cell debris, filtered through 45μm PVDF filters (Millipore # SLHVR33RS), and stored at -80˚C. Transductions were performed on semi-confluent wells in the presence of Polybrene (8μg/ml, Sigma #H9268) using spin-infection (800 x *g*, 37˚C, 90 minutes). Culture media containing selection antibiotics was added to transduced cultures 24 hours post-transduction.

Cloning of inducible CRISPRa-SunTag system components

To generate the plasmids for the inducible CRISPRa system, we re-engineered an existing CRISPRa technology [48] to enable Dox-inducible expression and independent component construct antibiotic selection. pCW-TRE, a Dox-inducible expression vector, was generated by modifying pCW-Cas9-Blast (a gift from Mohan Babu, Addgene # 83481) to include a single BamHI site. Next, the antibody component of the SunTag system (pHRdSV40-scFv-GCN4-sfGFP-VP64-GB1-NLS, a gift from Ron Vale, Addgene #60904) was digested with EcoRI+NotI and subcloned into the blunted BamHI site of pCW-TRE. The nuclease-inactive Cas9 fused to the SunTag scaffold (dCas9-SunTag derived from pHRdSV40-dCas9-10xGCN4_v4-P2A-BFP [48], a gift from Ron Vale, Addgene #60903) was assembled in-frame with a hygromycin resistance gene into pHR-PGK (a gift from Wendell Lim, Addgene #79120, [110]), generating pHR-PGK-dCas9-SunTag-P2A-HygR.

Generation of A549-SunTag and A549$^{\Delta STAT1}$-SunTag cells

To generate A549-SunTag and A549$^{\Delta STAT1}$-SunTag cells, we transduced A549 or A549$^{\Delta STAT1}$ cells with lentiviruses encoding the Dox-inducible transactivator component of SunTag (pCW-TRE-scFv-SunTag). Single cell clones were selected with Blasticidin (Fisher Scientific #BP264725, 1μg/ml). Next, pCW-TRE-scFv-SunTag single cell clones were transduced with lentiviruses encoding the SunTag nuclease-inactive Cas9 (pHR-PGK-dCas9-SunTag-P2A-HygR) and single cell clones were selected with Hygromycin (Thermo Scientific 10687010, 500μg/ml). Finally, multiple single cell clones of A549-SunTag and A549$^{\Delta STAT1}$-SunTag, selected for the expression of both components, were tested for gRNA-directed gene

activation capabilities with gRNAs targeting *CXCR4* and measuring *CXCR4* protein expression by flow cytometry as previously described [48].

Generation of ACE2 expressing cell lines

To generate ACE2-expressing A549 cell lines, the human ACE2 coding sequence (RefSeq accession NM_001371415.1) was PCR amplified and cloned into the BamHI site of lentiviral vector pHR-PGK (Addgene #79120). Lentivirus was produced as described above and used to transduce $5x10^4$ target cells (A549, $A549^{\Delta STAT1}$, A549-SunTag or $A549^{\Delta STAT1}$-SunTag) in 12 well plates. Single cell clones were expanded and validated for expression of ACE2 by Western Blot analysis (Abcam #ab15348).

qRT-PCR

For indicated experiments, A549 cultures were harvested by trypsinization, pelleted, and homogenized in Trizol (Invitrogen #15596026). Total RNA was isolated with the Direct-zol RNA MiniPrep kit (Zymo #R2050), including DNase protocol, according to manufacturer's instructions. For each sample, 1μg of total RNA was reverse transcribed (Applied Biosystems #4368814) with random hexamers for priming. qRT-PCR was performed with the TaqMan Universal Master Mix (Applied Biosystems #4440038), and TaqMan primer/probe sets for each gene of interest (*MX1*; Hs00895608_m1, *CD74*; Hs00269961_m1, *OAS1*; Hs00242 943_m1, *CTSS*; Hs00175407_m1, *GAPDH*; Hs99999905_m1). Ct values were used for calculation of gene expression using the comparative threshold cycle method [111] with *GAPDH* expression as loading control, comparing Dox^{on} condition to Dox^{off} condition.

SARS-CoV-2 infections

For validation studies employing gRNA or cDNA to express ISGs, indicated cells were plated 24 hours prior to infection. SARS-CoV-2 stocks were diluted in reduced serum DMEM (2% FBS) supplemented with 50mM HEPES and 1% PSN, inoculated to indicated cell cultures, and incubated at 37˚C for 1 hour. Infection medium was then replaced with DMEM (10% FBS and 1% PSN) for timepoints indicated in each experiment.

Methylene blue assay

A549-SunTag and $A549^{\Delta STAT1}$-SunTag cells were plated in 96-well plates (3000 cells/well, 4 replicates per condition, 1 plate for each time point) and infected with SARS-CoV-2. Infections were done in reduced serum DMEM (2% FBS, 50mM HEPES, 1% PSN), and virus was left on the cells for the indicated time points. Plates were fixed in 4% Paraformaldehyde at room temperature for a minimum of 24 hours. Cells were then washed twice with 100μl 0.1M sodium tetraborate (Sigma # 221732), stained with 0.5% methylene blue (Sigma # M9140) in 0.1M sodium tetraborate (15 minutes, room temperature), extensively washed in 0.1M sodium tetraborate, and extracted with 0.1M HCl. Absorbance was measured on a BioTek Cytation plate reader at 595 nm.

Curation and cloning of the ISG library

To assemble the list of ISGs targeted by the gRNA library, an established list of ISGs [3,4] was combined with a list of genes upregulated (RNA-Seq $\log_2$ fold-change >2, adjusted p value < 0.05) after 6 or 48 hours of IFN stimulation in A549 cells [53]. To focus the list on direct antiviral effectors, genes annotated as transcription factors [59], HLA genes, and central PRRs were excluded. gRNA sequences (n = 3 per gene) for the resulting 414 gene list were

selected from the Calabrese library [60]. The final gRNA library pool contained 1242 ISG-targeting gRNAs and 24 non-targeting controls. The gRNA library was synthesized as an oligonucleotide pool (Integrated DNA Technologies) and cloned into CROP-seq-opti (a gift from Jay Shendure, Addgene # 106280) [112] as described [113]. Briefly, the CROP-seq-opti backbone was digested with BsmBI and gel purified. 2000 fmoles of the gRNA library oligonucleotide pool were mixed with 50 fmoles of linearized CROP-seq-opti in 10μl of NEB-Builder master mix (New England Biolabs # E2621). After 1 hour incubation at 50˚C, the assembled plasmid pool was used to transform 25μl of electrocompetent bacteria (Lucigen #60242–2) on a Bio-Rad Gene-Pulser 2 electroporation system (Bio-Rad # 1652105) with the following settings: 25 μF, 200 Ohm, 1.5KV. Ampicillin resistant colonies were pooled, grown overnight in liquid culture (LB broth, Fisher BioReagents #BP1426) at 32˚C, and the plasmid library was extracted by Maxi prep (Qiagen #12362) according to the manufacturer's protocol. Plasmid library was packaged into lentiviruses and transducing units/ml (TU/ml) were determined by calculating colony forming units/ml of Puromycin (Sigma-Aldrich #P8833, 2μg/ml)-resistant transduced A549 cultures.

Inducible CRISPRa ISG screen for SARS-CoV-2 restriction factors

For each of 2 clones from each *STAT1* genotype (A549-SunTag ACE2 or A549$^{\Delta STAT1}$-SunTag ACE2, 2 clones each), 6 x 10^6 cells were transduced with gRNA library lentivirus (described above) at M.O.I. = 0.1, assuring zero or one gRNA/cell in more than 95% of library cells, and representation of 500 cells/gRNA. Transduced cultures were selected for CROP-seq-opti transduction with Puromycin (Sigma-Aldrich #P8833, 2μg/ml), and expanded for 14 days. 48 hours prior to SARS-COV-2 infection, gene expression was induced by treating the cells with Dox (5μg/ml). 2 x 10^6 cells (estimated representation of more that 1500 cells/gRNA) were infected with SARS-COV-2 (M.O.I. = 3). 72 hours post infection, after observation of significant CPE in infected cultures, genomic DNA was extracted from surviving cells for Illumina sequencing library preparation. In total, screens were conducted in two experiments, each experiment including two single cell clones from each *STAT1* genotype. In the first experiment, following infection, an additional 4ml of reduced-serum DMEM were added to the cultures, but the virus inoculum was not removed from culture wells. In the second experiment, the virus inoculum was removed from the cells after 1 hour of infection, cultures were washed twice with calcium/magnesium-free PBS, and cultured in DMEM (10% FBS) for 72 hours.

Screen library preparation and sequencing

CROP-seq-opti gRNA sequencing libraries were prepared as previously described [113]. Briefly, 100ng of each gDNA sample was PCR amplified in triplicate with Q5 High-Fidelity DNA Polymerase (NEB #M0494S) with 500nM primers (S4 Table) flanking the guide sequence cassette and including Illumina adaptor sequences and sample index sequences (98˚C x 30s, 98˚C x 10s, 72˚C x 45s, 25 cycles). PCR products were purified using 2.0X AMPure XP magnetic beads (Beckman Coulter #A63881) according to manufacturer's protocol. Sequencing libraries were quantified with the KAPA Library Quantification Kit (Roche #07960140001), pooled, and sequenced in multiplex on the Illumina NextSeq 500 platform using a 150-cycle mid output kit (Illumina # 20024904) with read configuration of 167 bases (read 1) and 8 bases (i7 index).

Inducible CRISPRa ISG screen data processing and analysis

Illumina BCL sequence files were converted to FASTQ format with the bcl2fastq tool (v2.20.0.422, Illumina). gRNA enrichment/depletion analyses were conducted with the

MAGeCK package (version 0.5.9.4, Wang *et al*., 2019). Sample x gRNA count tables and quality control matrixes were generated with the MAGeCK *count* function. Enrichment/depletion analyses were conducted with MAGeCK MLE for each *STAT1* genotype. To analyze gRNA enrichment, we used MAGeCK MLE with a design matrix generated by the R (version 4.0.2) *model.matrix()* function, with design formula specified as: ~(dox*virus) + experiment + clone. The resulting generalized linear model included factors for Dox status, SARS-CoV-2 infection status, clone, and experiment, as well as a dox:virus interaction term (used to test for gRNA enrichment/depletion by virus infection differences by dox status). MAGeCK MLE was run with 10 permutations, with normalization to NTG gRNAs. Enrichment/depletion p values were adjusted by the method of Benjamini and Hochberg within the MAGeCK MLE framework. To focus on genes enriched or depleted upon viral infection beyond potential virus-independent effects on library representation, we filtered to include hits with adjusted p value less than 0.1 for both SARS-CoV-2 infection status coefficient (Dox^{On} SARS-CoV-2 infected *vs* Dox^{On} mock infected) and the Dox status:SARS-CoV-2 infection status interaction term. "Antiviral"/"proviral" designations were made based on the sign of the β score for the SARS-CoV-2 infection status coefficient.

In analyses for antiproliferative/proapoptotic ISGs, hits were selected as adjusted p value less than 0.1 for the Dox status coefficient (Dox^{Off} mock infected *vs* Dox^{On} mock infected), and β score were multiplied by -1 to facilitate enrichment/depletion interpretation within the required model syntax.

Cloning procedures for individual guide RNAs

Cloning of individual gRNAs into CROP-seq-opti vectors was performed as previously described [113,114]. Briefly, for targeted (i.e. non-library) CRISPRa experiments, gRNA sequences were synthesized (Integrated DNA technologies) as oligonucleotide duplexes with BsmBI-compatible overhangs. CROP-seq-opti (Addgene # 106280) was linearized by BsmBI (New England Biolabs # R0580S) digestion. Oligonucleotides were phosphorylated with T4 polynucleotide kinase (New England Biolabs #M0201L), annealed and ligated (Quick Ligation kit, New England Biolabs #M2200S) into BsmBI digested CROP-seq-opti. 2μl from the ligation reaction were used for transformation of 10μl of NEB stable competent E. coli cells (C3040, New England Biolabs # C3040H). Proper insertion of gRNA sequence was confirmed by Sanger sequencing primed from the U6 promoter region.

Cloning procedures for ISG cDNA ORFs

To clone screen hit cDNAs for validation experiments, the complete coding sequences of canonical isoforms (annotated by Uniprot; [115]) of candidate genes were either synthesized as gBlocks (Integrated DNA Technologies) or PCR amplified from cDNA derived from IFNα2b-treated A549 cells. Genetic sequences were synthesized/amplified with homology overhangs complementary to the overhangs of EcoRI+BamHI digested pLVX-TetOne-Puro (Takara # 631849). 100ng of cDNA were ligated into 75ng of gel-purified digested vector using Neb builder (New England Biolabs #E2621) in a final reaction volume of 10μl. Ampicillin resistant colonies were grown overnight in LB media at 30˚C, and plasmids were extracted by Mini prep (Qiagen # 27106) according to the manufacturer's protocol.

Flow cytometry

For VSV-GFP experiments, cells were fixed with 4% Paraformaldehyde for 30 minutes at room temperature and analyzed for GFP fluorescence on a Gallios flow cytometer (Beckman-Coulter). For SARS-CoV-2 experiments, cells were fixed with 4% paraformaldehyde at room

temperature for a minimum of 24 hours, washed once with PBS and permeabilized with 1X perm-wash buffer (BDBiosciences #554723) for 5 minutes. AlexaFluor 647-conjugated SARS-CoV nucleocapsid (N) antibody (clone 1C7C7, generously provided by the Center for Therapeutic Antibody Discovery at the Icahn School of Medicine at Mount Sinai) was diluted 1:400 in perm-wash buffer, and added directly to permeabilized samples, which were then incubated at room temperature for 40 minutes in the dark. Samples were washed once with 1X perm-wash buffer, once with calcium/magnesium-free PBS, and acquired on a Gallios flow cytometer (Beckman-Coulter). For all viral infections, analysis was performed with FlowJo software (Version 10.7.1, Becton Dickinson), excluding cell doublets and debris and gating according to mock infected populations (S6 Fig). Samples with fewer than 2000 cell events after doublet and debris gating were excluded from analysis.

Immunoblotting

Cells were lysed in ice-cold RIPA buffer (ThermoFisher scientific # 89900) supplemented with protease inhibitor cocktail (Roche # 11697498001) for 30 minutes on ice and clarified by centrifugation (21,000 *g* x 15 minutes, 4C). Protein amounts were quantified using the Pierce BCA assay (Pierce # 23225). 20–40μg protein were separated by sodium dodecyl sulfate–polyacrylamide gel electrophoresis (SDS-PAGE) using a 4–12% gradient gel (ThermoFisher Scientific # NW04125BOX), and transferred to a nitrocellulose membrane (ThermoFisher Scientific # IB23001) according to the manufacturer instructions. Membranes were blocked for 1 hour at room temperature with 5% skim milk (Difco # DF0032-17-3) in Tween Tris-Buffered Saline (TBST; ThermoFisher Scientific # PI28358), and blotted with primary antibodies overnight at 4C with gentle agitation. After excessive washing in TBST, membranes were incubated for 1 hour at room temperature with HRP-conjugated secondary antibody. HRP signal was detected using an enhanced chemiluminescence substrate (Pierce # 32106) in a ChemiDoc imaging system (BioRad # 1708265). Antibodies used: Rabbit anti-CTSS (Cell Signaling Technologies, CST # 25084); Rabbit anti-CD74 (CST # 77274); Rabbit anti-OAS2 (CST # 24344); Rabbit anti-OAS3 (CST # 41440); all in 1:1000 dilution in blocking solution. Rabbit anti-OAS1 (CST # 14498) was diluted 1:500. Rabbit anti-OASL (GeneTex # GTX31572) was used at 1:1000 dilution in blocking solution. Rabbit anti-GAPDH was used for loading control (Abcam # ab9485) was diluted 1:10,000. Secondary HRP-conjugated anti-rabbit (CST # 7074S) was diluted 1:2000 in blocking buffer.

Immunofluorescence high throughput microscopy

SARS-CoV-2 infected A549-SunTag ACE2 and A549$^{\Delta STAT1}$-SunTag ACE2 in 96-well plates were fixed with 4% Paraformaldehyde at room temperature for a minimum 24 hours, washed with PBS, and permeabilized with 0.1% Triton X-100 (Thermo Scientific #327371000) for 15 minutes. Plates were blocked with 3% Bovine serum albumin (BSA, Miltenyi Biotec #130-091-376) in PBS for 1 hour. AlexaFluor 647-conjugated SARS-CoV nucleocapsid (N) antibody (clone 1C7C7) was diluted 1:2000 in 0.5% BSA in PBS and added to wells for 1 hour incubation. Samples were then washed twice with PBS and stained with 4′,6-diamidino-2-phenylindole (DAPI, Thermo Scientific #D1306) diluted 1:200 in 0.5% BSA in PBS. All steps were done at room temperature. Plates were imaged on a Celigo instrument (Nexcelom Biosciences) and the fraction of infected cells per well was determined using CellProfiler [116].

SARS-CoV-2 growth curves by plaque assay

A549$^{\Delta STAT1}$ SunTag cells, expressing gRNAs targeting either *OAS1* or NTG, were pretreated, or not, with Dox (5μg/ml, 48 hours before infection), and infected with SARS-CoV-2 (M.O.I.

= 0.1). After 1 hour, virus inoculum was removed and replaced with DMEM/10% FBS supplemented with or without Dox. Every 24 hours post infection, 100μl of the culture supernatants was collected, serially diluted, and used to infect $2x10^5$ Vero-E6 cells plated in a 24 well plates (37˚C, agitating every 10 minutes). After 1 hour, inoculum was removed and replaced with overlay media consisting of Minimum Essential Media (MEM, Thermo # 11095080) supplemented with 0.8% SeaPlaque Agarose (Lonza # 50104), 4% FBS and 1% PSN pre-warmed to 37˚. At 72 hours post-infection, Vero-E6 cells were fixed in 4% Paraformaldehyde at room temperature for 24 hours, washed twice with PBS and stained with 1% Crystal violet (Sigma # C0775) for 15 minutes. Viral titer was determined by calculating infectious units/ml.

Quantification and statistical analysis

Unless otherwise indicated, error bars indicate standard deviation from the mean (SD) of at least 3 biological replicates (repeats of identical experiments, conducted independently). For flow cytometry and immunofluorescence experiments, statistical significance was determined with one-sided paired ratio Student's t-test, with p values < 0.05 considered to be significant (S6 Table contains exact p-values for all experiments).

Supporting information

S1 Fig. Inducible CRISPRa ISG screen optimization and quality control. (A) Pilot experiment using Methylene Blue assay to assess SARS-CoV-2 CPE under different infection conditions. A549-SunTag ACE2 and $A549^{\Delta STAT1}$-SunTag ACE2 cells, expressing *LY6E* gRNA or a non-targeting gRNA (NTG) were infected with SARS-CoV-2 at indicated M.O.I., fixed at indicated time points, and stained with methylene blue. Values indicate percent OD595 absorption relative to time point = 0 (set to 100%). **(B)** CRISPRa screen quality metrics: sequencing reads per sample. Values indicate number of reads sequenced for each sample in the pooled screens. Percentage values (light fill) for reads that fail to map to gRNA sequences in the ISG library reference. **(C)** CRISPRa screen quality metrics: Normalized read count distribution per sample. Log_{10} transformed read count for each sample normalized to the count of non-targeting guides.
(TIF)

S2 Fig. Comparisons to other ISG-focused screen results. (A) Venn diagram generated from intersecting lists of ISGs from the libraries of Wickenhagen *et al.* [31], Martin-Sancho *et al.* [29] and our ISG library. **(B)** Similar to A, highlighting shared and distinct antiviral hits. **(C)** Comparison of candidate antiviral hits from published studies and this study. Z scores of infections were calculated from published datasets and ranked. Black square: antiviral hit. White square: not antiviral hit. Empty square: not tested/no data available.
(TIF)

S3 Fig. Complete validation results of screen hits tested in targeted CRISPRa studies. (A) qRT-PCR analysis demonstrates effective CRISPRa gene induction in A549-SunTag ACE2 cells. Values indicate fold change expression (Dox^{on} relative to Dox^{off}) for indicated genes (*CD74*, *OAS1* and *CTSS*) in A549-SunTag ACE2 cells expressing either corresponding gRNA or NTG. Fold change values calculated using the ΔΔCt method with GAPDH as normalization control. Undetectable Ct value for Dox^{off} condition of cells expressing NTG and probed for *CD74* expression was set to 40 to enable fold change calculation. **(B)** qRT-PCR mean threshold cycle (Ct) values for *CD74*, *OAS1*, *CTSS* and *GAPDH* in A549-SunTag ACE2 cells expressing gRNA against gene of interest (GOI, circle) or NTG (diamond) in Dox^{on} and Dox^{off} cells. Error bars indicate ± SD Ct value. **(C)** Representative flow cytometry histograms for

SARS-CoV-2 N protein in A549-SunTag ACE2 and A549$^{\Delta STAT1}$-SunTag ACE2 transduced with indicated gRNAs, treated (red) or not treated (gray) with Dox, at 24 hours post-infection with SARS-CoV-2 (M.O.I. = 2). **(D)** Percent of infected (SARS-CoV-2 N protein positive) cells quantified across biological replicates (n = 3) for experiments described in (C). Values denote percent of infected cells in Dox^{on} cultures relative to paired Dox^{off} cultures. Points represent individual biological replicates, black lines indicate mean values of biological replicates for each indicated ISG gRNA. Red points indicate statistical significance ($p < 0.05$) as determined by paired ratio Student's t-test. **(E)** Representative immunofluorescence images for SARS-CoV-2 N protein and DAPI in A549-SunTag ACE2 and A549$^{\Delta STAT1}$-SunTag ACE2 transduced with indicated gRNAs and treated with Dox, at 72 hours post-infection with SARS-CoV-2 (M.O.I. = 2). **(F)** Percent of infected (SARS-CoV-2 N protein positive) cells quantified across biological replicates for experiments described in (E). Values denote percent of infected cells in Dox^{on} cultures relative to paired Dox^{off} cultures. Points represent individual biological replicates, black lines indicate mean values of biological replicates for each indicated ISG gRNA. Statistical significance as in (D).
(TIF)

S4 Fig. Protein expression patterns of representative ISGs by cDNA or CRISPRa. (A-B) Immunoblot analysis of CD74 **(A)** and Cathepsin S **(B)** expression in A549-ACE2 cells transduced with lentivirus encoding indicated ORFs compared to A549-SunTag ACE2 cells expressing guides targeting the activation of *CD74*, *CTSS* or a non-targeting guide. Cells were incubated with Dox to induce gene expression for 48 hours prior to processing for immunoblot analysis with the indicated antibodies.
(TIF)

S5 Fig. Inducible CRISPRa ISG screen highlights ISGs with putative antiproliferative/proapoptotic effects. (A) ISGs ranked by the inverse of their β-scores for the Dox status coefficient (Dox^{Off} mock infected *vs* Dox^{On} mock infected). Significantly (adjusted p value < 0.1) enriched/depleted gRNAs are highlighted in green/purple respectively. **(B)** Venn diagram of significantly depleted (i.e. candidate antiproliferative/proapoptotic) ISG hits from (A) in A549-SunTag ACE2 and A549$^{\Delta STAT1}$-SunTag ACE2 screens.
(TIF)

S6 Fig. Gating strategy for flow cytometry experiments. Representative gating strategy for identifying SARS-CoV-2 infected cells.
(TIF)

S1 Table. ISGs in screening library.
(XLSX)

S2 Table. ISG guide RNA sequences.
(XLSX)

S3 Table. ISG screen results: MAGeCK-MLE output.
(XLSX)

S4 Table. Oligonucleotide sequences.
(XLSX)

S5 Table. ISGs with putative antiproliferative effects.
(XLSX)

S6 Table. Validation experiment statistical testing p values.
(XLSX)

Acknowledgments

We thank Mayte Suarez-Farinas for advice on statistics and experimental design, and Thomas Moran, Center for Therapeutic Antibody Discovery at the Icahn School of Medicine at Mount Sinai, for kindly providing anti-SARS-CoV Nucleocapsid antibody. We thank Meike Dittmann for $A549^{\Delta STAT1}$ cell lines, Benjamin R. tenOever and Skyler Uhl for technical assistance with plaque assays, and Michael A. Schotsaert for flow cytometry support. We also thank Randy Albrecht for BSL3 facility management and support. We thank Dusan Bogunovic and Ivan Marazzi for discussion, helpful advice, and critical reading of the manuscript. We thank all members of the Rosenberg lab for advice and support. Figure panels Figs 1A and 2A were created with BioRender.com.

Author Contributions

Conceptualization: Oded Danziger, Brad R. Rosenberg.

Data curation: Oded Danziger, Brad R. Rosenberg.

Formal analysis: Oded Danziger, Roosheel S. Patel, Brad R. Rosenberg.

Funding acquisition: Brad R. Rosenberg.

Investigation: Oded Danziger, Roosheel S. Patel, Emma J. DeGrace, Mikaela R. Rosen.

Methodology: Oded Danziger, Brad R. Rosenberg.

Project administration: Brad R. Rosenberg.

Supervision: Brad R. Rosenberg.

Validation: Oded Danziger, Roosheel S. Patel.

Visualization: Oded Danziger, Roosheel S. Patel, Brad R. Rosenberg.

Writing – original draft: Oded Danziger, Roosheel S. Patel, Brad R. Rosenberg.

Writing – review & editing: Oded Danziger, Roosheel S. Patel, Brad R. Rosenberg.

References

1. Schneider WM, Chevillotte MD, Rice CM. Interferon-stimulated genes: a complex web of host defenses. Annu Rev Immunol. 2014; 32: 513–45. https://doi.org/10.1146/annurev-immunol-032713-120231 PMID: 24555472
2. Schoggins JW. Interferon-Stimulated Genes: What Do They All Do? Annu Rev Virol. 2019; 6: 567–584. https://doi.org/10.1146/annurev-virology-092818-015756 PMID: 31283436
3. Schoggins JW, Wilson SJ, Panis M, Murphy MY, Jones CT, Bieniasz P, et al. A diverse range of gene products are effectors of the type I interferon antiviral response. Nature. 2011; 472: 481–5. https://doi.org/10.1038/nature09907 PMID: 21478870
4. Schoggins JW, MacDuff DA, Imanaka N, Gainey MD, Shrestha B, Eitson JL, et al. Pan-viral specificity of IFN-induced genes reveals new roles for cGAS in innate immunity. Nature. 2014; 505: 691–695. https://doi.org/10.1038/nature12862 PMID: 24284630
5. Dittmann M, Hoffmann HH, Scull MA, Gilmore RH, Bell KL, Ciancanelli M, et al. A serpin shapes the extracellular environment to prevent influenza a virus maturation. Cell. 2015; 160: 631–643. https://doi.org/10.1016/j.cell.2015.01.040 PMID: 25679759
6. Perelman SS, Abrams ME, Eitson JL, Chen D, Jimenez A, Mettlen M, et al. Cell-Based Screen Identifies Human Interferon-Stimulated Regulators of Listeria monocytogenes Infection. PLoS Pathog. 2016; 12. https://doi.org/10.1371/journal.ppat.1006102 PMID: 28002492

7. Feng J, Wickenhagen A, Turnbull ML, Rezelj V V., Kreher F, Tilston-Lunel NL, et al. Interferon-Stimulated Gene (ISG)-Expression Screening Reveals the Specific Antibunyaviral Activity of ISG20. Jung JU, editor. J Virol. 2018;92. https://doi.org/10.1128/JVI.02140-17 PMID: 29695422

8. Schmitt MJ, Philippidou D, Reinsbach SE, Margue C, Wienecke-Baldacchino A, Nashan D, et al. Interferon-γ-induced activation of Signal Transducer and Activator of Transcription 1 (STAT1) up-regulates the tumor suppressing microRNA-29 family in melanoma cells. Cell Commun Signal. 2012; 10: 41. https://doi.org/10.1186/1478-811X-10-41 PMID: 23245396

9. Rosebeck S, Leaman DW. Mitochondrial localization and pro-apoptotic effects of the interferon-inducible protein ISG12a. Apoptosis. 2008; 13: 562–572. https://doi.org/10.1007/s10495-008-0190-0 PMID: 18330707

10. Francois-Newton V, Livingstone M, Payelle-Brogard B, Uzé G, Pellegrini S. USP18 establishes the transcriptional and anti-proliferative interferon α/β differential. Biochem J. 2012; 446: 509–516. https://doi.org/10.1042/BJ20120541 PMID: 22731491

11. Brzostek-Racine S, Gordon C, Van Scoy S, Reich NC. The DNA Damage Response Induces IFN. J Immunol. 2011; 187: 5336–5345. https://doi.org/10.4049/jimmunol.1100040 PMID: 22013119

12. Stertz S, Hale BG. Interferon system deficiencies exacerbating severe pandemic virus infections. Trends Microbiol. 2021; 1–10. https://doi.org/10.1016/j.tim.2021.03.001 PMID: 33757684

13. Miorin L, Kehrer T, Sanchez-Aparicio MT, Zhang K, Cohen P, Patel RS, et al. SARS-CoV-2 Orf6 hijacks Nup98 to block STAT nuclear import and antagonize interferon signaling. Proc Natl Acad Sci U S A. 2020; 117: 28344–28354. https://doi.org/10.1073/pnas.2016650117 PMID: 33097660

14. Lokugamage KG, Hage A, de Vries M, Valero-Jimenez AM, Schindewolf C, Dittmann M, et al. Type I Interferon Susceptibility Distinguishes SARS-CoV-2 from SARS-CoV. J Virol. 2020;94. https://doi.org/10.1128/jvi.01410-20 PMID: 32938761

15. Lei X, Dong X, Ma R, Wang W, Xiao X, Tian Z, et al. Activation and evasion of type I interferon responses by SARS-CoV-2. Nat Commun. 2020;11. https://doi.org/10.1038/s41467-019-13872-1 PMID: 31896763

16. Mantlo E, Bukreyeva N, Maruyama J, Paessler S, Huang C. Antiviral activities of type I interferons to SARS-CoV-2 infection. Antiviral Res. 2020;179. https://doi.org/10.1016/j.antiviral.2020.104811 PMID: 32360182

17. Blanco-Melo D, Nilsson-Payant BE, Liu WC, Uhl S, Hoagland D, Møller R, et al. Imbalanced Host Response to SARS-CoV-2 Drives Development of COVID-19. Cell. 2020; 181: 1036–1045.e9. https://doi.org/10.1016/j.cell.2020.04.026 PMID: 32416070

18. Lee JS, Park S, Jeong HW, Ahn JY, Choi SJ, Lee H, et al. Immunophenotyping of COVID-19 and influenza highlights the role of type I interferons in development of severe COVID-19. Sci Immunol. 2020; 5: eabd1554. https://doi.org/10.1126/sciimmunol.abd1554 PMID: 32651212

19. Zhou Z, Ren L, Zhang L, Zhong J, Xiao Y, Jia Z, et al. Heightened Innate Immune Responses in the Respiratory Tract of COVID-19 Patients. Cell Host Microbe. 2020; 27: 883–890.e2. https://doi.org/10.1016/j.chom.2020.04.017 PMID: 32407669

20. Park A, Iwasaki A. Type I and Type III Interferons—Induction, Signaling, Evasion, and Application to Combat COVID-19. Cell Host Microbe. 2020; 27: 870–878. https://doi.org/10.1016/j.chom.2020.05.008 PMID: 32464097

21. Bastard P, Rosen LB, Zhang Q, Michailidis E, Hoffmann H-H, Zhang Y, et al. Autoantibodies against type I IFNs in patients with life-threatening COVID-19. Science. 2020; 370: eabd4585. https://doi.org/10.1126/science.abd4585 PMID: 32972996

22. Troya J, Bastard P, Planas-Serra L, Ryan P, Ruiz M, de Carranza M, et al. Neutralizing Autoantibodies to Type I IFNs in >10% of Patients with Severe COVID-19 Pneumonia Hospitalized in Madrid, Spain. J Clin Immunol. 2021. https://doi.org/10.1007/s10875-021-01036-0 PMID: 33851338

23. van der Wijst MGP, Vazquez SE, Hartoularos GC, Bastard P, Grant T, Bueno R, et al. Longitudinal single-cell epitope and RNA-sequencing reveals the immunological impact of type 1 interferon autoantibodies in critical COVID-19. bioRxiv Prepr Serv Biol. 2021. https://doi.org/10.1101/2021.03.09.434529 PMID: 33758859

24. Bastard P, Orlova E, Sozaeva L, Lévy R, James A, Schmitt MM, et al. Preexisting autoantibodies to type I IFNs underlie critical COVID-19 pneumonia in patients with APS-1. J Exp Med. 2021;218. https://doi.org/10.1084/jem.20210554 PMID: 33890986

25. Broggi A, Ghosh S, Sposito B, Spreafico R, Balzarini F, Lo Cascio A, et al. Type III interferons disrupt the lung epithelial barrier upon viral recognition. Science. 2020; 369: 706–712. https://doi.org/10.1126/science.abc3545 PMID: 32527925

26. Pfaender S, Mar KB, Michailidis E, Kratzel A, Boys IN, V'kovski P, et al. LY6E impairs coronavirus fusion and confers immune control of viral disease. Nat Microbiol. 2020; 5: 1330–1339. https://doi.org/10.1038/s41564-020-0769-y PMID: 32704094

27. Bruchez A, Sha K, Johnson J, Chen L, Stefani C, McConnell H, et al. MHC class II transactivator CIITA induces cell resistance to Ebola virus and SARS-like coronaviruses. Science. 2020; 370: 241–247. https://doi.org/10.1126/science.abb3753 PMID: 32855215

28. Neil SJD, Zang T, Bieniasz PD. Tetherin inhibits retrovirus release and is antagonized by HIV-1 Vpu. Nature. 2008; 451: 425–430. https://doi.org/10.1038/nature06553 PMID: 18200009

29. Martin-Sancho L, Lewinski MK, Pache L, Stoneham CA, Yin X, Becker ME, et al. Functional Landscape of SARS-CoV-2 Cellular Restriction. Mol Cell. 2021. https://doi.org/10.1016/j.molcel.2021.04.008 PMID: 33930332

30. Lee S, Lee Y suk, Choi Y, Son A, Park, Lee KM, et al. The SARS-CoV-2 RNA interactome. Mol Cell. 2021; 81: 2838–2850.e6. https://doi.org/10.1016/j.molcel.2021.04.022 PMID: 33989516

31. Wickenhagen A, Sugrue E, Lytras S, Kuchi S, Noerenberg M, Turnbull ML, et al. A prenylated dsRNA sensor protects against severe COVID-19. Science. 2021; 374: eabj3624. https://doi.org/10.1126/science.abj3624 PMID: 34581622

32. Soveg FW, Schwerk J, Gokhale NS, Cerosaletti K, Smith JR, Pairo-Castineira E, et al. Endomembrane targeting of human OAS1 p46 augments antiviral activity. Elife. 2021;10. https://doi.org/10.7554/eLife.71047 PMID: 34342578

33. Kuroda M, Halfmann PJ, Hill-Batorski L, Ozawa M, Lopes TJS, Neumann G, et al. Identification of interferon-stimulated genes that attenuate Ebola virus infection. Nat Commun. 2020; 11: 2953. https://doi.org/10.1038/s41467-020-16768-7 PMID: 32528005

34. Kane M, Zang TM, Rihn SJ, Zhang F, Kueck T, Alim M, et al. Identification of Interferon-Stimulated Genes with Antiretroviral Activity. Cell Host Microbe. 2016; 20: 392–405. https://doi.org/10.1016/j.chom.2016.08.005 PMID: 27631702

35. Prelich G. Gene overexpression: Uses, mechanisms, and interpretation. Genetics. 2012; 190: 841–854. https://doi.org/10.1534/genetics.111.136911 PMID: 22419077

36. Villalón-Letelier F, Brooks AG, Saunders PM, Londrigan SL, Reading PC. Host cell restriction factors that limit influenza a infection. Viruses. 2017; 9: 1–18. https://doi.org/10.3390/v9120376 PMID: 29215570

37. Bonnevie-Nielsen V, Field LL, Lu S, Zheng DJ, Li M, Martensen PM, et al. Variation in antiviral 2′,5′-oligoadenylate synthetase (2′5′AS) enzyme activity is controlled by a single-nucleotide polymorphism at a splice-acceptor site in the OAS1 gene. Am J Hum Genet. 2005; 76: 623–633. https://doi.org/10.1086/429391 PMID: 15732009

38. Carey CM, Govande AA, Cooper JM, Hartley MK, Kranzusch PJ, Elde NC. Recurrent Loss-of-Function Mutations Reveal Costs to OAS1 Antiviral Activity in Primates. Cell Host Microbe. 2019; 25: 336–343.e4. https://doi.org/10.1016/j.chom.2019.01.001 PMID: 30713099

39. Kerns JA, Emerman M, Malik HS. Positive selection and increased antiviral activity associated with the PARP-containing isoform of human zinc-finger antiviral protein. PLoS Genet. 2008; 4: 0150–0158. https://doi.org/10.1371/journal.pgen.0040021 PMID: 18225958

40. Blondel D, Kheddache S, Lahaye X, Dianoux L, Chelbi-Alix MK. Resistance to Rabies Virus Infection Conferred by the PMLIV Isoform. J Virol. 2010; 84: 10719–10726. https://doi.org/10.1128/JVI.01286-10 PMID: 20702643

41. Pestal K, Funk CC, Snyder JM, Price ND, Treuting PM, Stetson DB. Isoforms of RNA-Editing Enzyme ADAR1 Independently Control Nucleic Acid Sensor MDA5-Driven Autoimmunity and Multi-organ Development. Immunity. 2015; 43: 933–944. https://doi.org/10.1016/j.immuni.2015.11.001 PMID: 26588779

42. Konermann S, Brigham MD, Trevino AE, Joung J, Abudayyeh OO, Barcena C, et al. Genome-scale transcriptional activation by an engineered CRISPR-Cas9 complex. Nature. 2015; 517: 583–588. https://doi.org/10.1038/nature14136 PMID: 25494202

43. Heaton BE, Kennedy EM, Dumm RE, Harding AT, Sacco MT, Sachs D, et al. A CRISPR Activation Screen Identifies a Pan-avian Influenza Virus Inhibitory Host Factor. Cell Rep. 2017; 20: 1503–1512. https://doi.org/10.1016/j.celrep.2017.07.060 PMID: 28813663

44. Dukhovny A, Lamkiewicz K, Chen Q, Fricke M, Jabrane-Ferrat N, Marz M, et al. A CRISPR Activation Screen Identifies Genes That Protect against Zika Virus Infection. J Virol. 2019; 93: 1–16. https://doi.org/10.1128/JVI.00211-19 PMID: 31142663

45. Luu AP, Yao Z, Ramachandran S, Azzopardi SA, Miles LA, Schneider WM, et al. A CRISPR Activation Screen Identifies an Atypical Rho GTPase That Enhances Zika Viral Entry. Viruses. 2021; 13: 2113. https://doi.org/10.3390/v13112113 PMID: 34834920

46. Biering SB, Sarnik SA, Wang E, Zengel JR, Sathyan V, Nguyenla X, et al. Genome-wide, bidirectional CRISPR screens identify mucins as critical host factors modulating SARS-CoV-2 infection. bioRxiv. 2021; 2021.04.22.440848. https://doi.org/10.1101/2021.04.22.440848

47. Goujon C, Rebendenne A, Roy P, Bonaventure B, Valadao AC, Desmarets L, et al. Bidirectional genome-wide CRISPR screens reveal host factors regulating SARS-CoV-2, MERS-CoV and seasonal HCoVs. bioRxiv. 2021; 2021.05.19.444823. https://doi.org/10.21203/rs.3.rs-555275/v1 PMID: 34075371

48. Tanenbaum ME, Gilbert LA, Qi LS, Weissman JS, Vale RD. A protein-tagging system for signal amplification in gene expression and fluorescence imaging. Cell. 2014; 159: 635–46. https://doi.org/10.1016/j.cell.2014.09.039 PMID: 25307933

49. Han J, Perez JT, Chen C, Li Y, Benitez A, Kandasamy M, et al. Genome-wide CRISPR/Cas9 Screen Identifies Host Factors Essential for Influenza Virus Replication. Cell Rep. 2018; 23: 596–607. https://doi.org/10.1016/j.celrep.2018.03.045 PMID: 29642015

50. Li B, Clohisey SM, Chia BS, Wang B, Cui A, Eisenhaure T, et al. Genome-wide CRISPR screen identifies host dependency factors for influenza A virus infection. Nat Commun. 2020; 11: 164. https://doi.org/10.1038/s41467-019-13965-x PMID: 31919360

51. Blanchard EL, Vanover D, Bawage SS, Tiwari PM, Rotolo L, Beyersdorf J, et al. Treatment of influenza and SARS-CoV-2 infections via mRNA-encoded Cas13a in rodents. Nat Biotechnol. 2021. https://doi.org/10.1038/s41587-021-00822-w PMID: 33536629

52. Cheon H, Borden EC, Stark GR. Interferons and their stimulated genes in the tumor microenvironment. Semin Oncol. 2014; 41: 156–173. https://doi.org/10.1053/j.seminoncol.2014.02.002 PMID: 24787290

53. Seifert LL, Si C, Saha D, Sadic M, de Vries M, Ballentine S, et al. The ETS transcription factor ELF1 regulates a broadly antiviral program distinct from the type I interferon response. Fujita T, editor. PLOS Pathog. 2019; 15: e1007634. https://doi.org/10.1371/journal.ppat.1007634 PMID: 31682641

54. Turan K, Mibayashi M, Sugiyama K, Saito S, Numajiri A, Nagata K. Nuclear MxA proteins form a complex with influenza virus NP and inhibit the transcription of the engineered influenza virus genome. Nucleic Acids Res. 2004; 32: 643–652. https://doi.org/10.1093/nar/gkh192 PMID: 14752052

55. Speer SD, Li Z, Buta S, Payelle-Brogard B, Qian L, Vigant F, et al. ISG15 deficiency and increased viral resistance in humans but not mice. Nat Commun. 2016; 7: 11496. https://doi.org/10.1038/ncomms11496 PMID: 27193971

56. Kumar A, Commane M, Flickinger TW, Horvath CM, Stark GR. Defective TNF-alpha-induced apoptosis in STAT1-null cells due to low constitutive levels of caspases. Science. 1997; 278: 1630–2. https://doi.org/10.1126/science.278.5343.1630 PMID: 9374464

57. Stojdl DF, Lichty BD, TenOever BR, Paterson JM, Power AT, Knowles S, et al. VSV strains with defects in their ability to shutdown innate immunity are potent systemic anti-cancer agents. Cancer Cell. 2003; 4: 263–275. https://doi.org/10.1016/s1535-6108(03)00241-1 PMID: 14585354

58. DeWeirdt PC, Sangree AK, Hanna RE, Sanson KR, Hegde M, Strand C, et al. Genetic screens in isogenic mammalian cell lines without single cell cloning. Nat Commun. 2020; 11: 752. https://doi.org/10.1038/s41467-020-14620-6 PMID: 32029722

59. Lambert SA, Jolma A, Campitelli LF, Das PK, Yin Y, Albu M, et al. The Human Transcription Factors. Cell. 2018; 172: 650–665. https://doi.org/10.1016/j.cell.2018.01.029 PMID: 29425488

60. Sanson KR, Hanna RE, Hegde M, Donovan KF, Strand C, Sullender ME, et al. Optimized libraries for CRISPR-Cas9 genetic screens with multiple modalities. Nat Commun. 2018; 9: 1–15. https://doi.org/10.1038/s41467-017-02088-w PMID: 29317637

61. Wang B, Wang M, Zhang W, Xiao T, Chen CH, Wu A, et al. Integrative analysis of pooled CRISPR genetic screens using MAGeCKFlute. Nat Protoc. 2019; 14: 756–780. https://doi.org/10.1038/s41596-018-0113-7 PMID: 30710114

62. Li W, Köster J, Xu H, Chen CH, Xiao T, Liu JS, et al. Quality control, modeling, and visualization of CRISPR screens with MAGeCK-VISPR. Genome Biol. 2015; 16: 1–13. https://doi.org/10.1186/s13059-014-0572-2 PMID: 25583448

63. Shi G, Kenney AD, Kudryashova E, Zani A, Zhang L, Lai KK, et al. Opposing activities of IFITM proteins in SARS-CoV-2 infection. EMBO J. 2021; 40: 1–12. https://doi.org/10.15252/embj.2020106501 PMID: 33270927

64. Simmons G, Gosalia DN, Rennekamp AJ, Reeves JD, Diamond SL, Bates P. Inhibitors of cathepsin L prevent severe acute respiratory syndrome coronavirus entry. Proc Natl Acad Sci U S A. 2005; 102: 11876–11881. https://doi.org/10.1073/pnas.0505577102 PMID: 16081529

65. Herbig U, Jobling WA, Chen BPC, Chen DJ, Sedivy JM. Telomere shortening triggers senescence of human cells through a pathway involving ATM, p53, and p21CIP1, but not p16INK4a. Mol Cell. 2004; 14: 501–513. https://doi.org/10.1016/s1097-2765(04)00256-4 PMID: 15149599

66. Walczak H, Degli-Esposti MA, Johnson RS, Smolak PJ, Waugh JY, Boiani N, et al. TRAIL-R2: A novel apoptosis-mediating receptor for TRAIL. EMBO J. 1997; 16: 5386–5397. https://doi.org/10.1093/emboj/16.17.5386 PMID: 9311998

67. Yuan X, Wu J, Shan Y, Yao Z, Dong B, Chen B, et al. SARS coronavirus 7a protein blocks cell cycle progression at G0/G1 phase via the cyclin D3/pRb pathway. Virology. 2006; 346: 74–85. https://doi.org/10.1016/j.virol.2005.10.015 PMID: 16303160

68. Zimmer MM, Kibe A, Rand U, Pekarek L, Ye L, Buck S, et al. The short isoform of the host antiviral protein ZAP acts as an inhibitor of SARS-CoV-2 programmed ribosomal frameshifting. Nat Commun. 2021; 12: 7193. https://doi.org/10.1038/s41467-021-27431-0 PMID: 34893599

69. Nchioua R, Kmiec D, Müller JA, Conzelmann C, Groß R, Swanson CM, et al. SARS-CoV-2 Is Restricted by Zinc Finger Antiviral Protein despite Preadaptation to the Low-CpG Environment in Humans. Luban J, Goff SP, editors. MBio. 2020;11. https://doi.org/10.1128/mBio.01930-20 PMID: 33067384

70. Gack MU, Shin YC, Joo CH, Urano T, Liang C, Sun L, et al. TRIM25 RING-finger E3 ubiquitin ligase is essential for RIG-I-mediated antiviral activity. Nature. 2007; 446: 916–920. https://doi.org/10.1038/nature05732 PMID: 17392790

71. Schröder B. The multifaceted roles of the invariant chain CD74—More than just a chaperone. Biochim Biophys Acta. 2016; 1863: 1269–81. https://doi.org/10.1016/j.bbamcr.2016.03.026 PMID: 27033518

72. Assis DN, Leng L, Du X, Zhang CK, Grieb G, Merk M, et al. The role of macrophage migration inhibitory factor in autoimmune liver disease. Hepatology. 2014; 59: 580–91. https://doi.org/10.1002/hep.26664 PMID: 23913513

73. Schwartz SL, Conn GL. RNA regulation of the antiviral protein 2′-5′-oligoadenylate synthetase. Wiley Interdiscip Rev RNA. 2019; 10: e1534. https://doi.org/10.1002/wrna.1534 PMID: 30989826

74. Hornung V, Hartmann R, Ablasser A, Hopfner KP. OAS proteins and cGAS: Unifying concepts in sensing and responding to cytosolic nucleic acids. Nat Rev Immunol. 2014; 14: 521–528. https://doi.org/10.1038/nri3719 PMID: 25033909

75. Zhu J, Zhang Y, Ghosh A, Cuevas RA, Forero A, Dhar J, et al. Antiviral Activity of Human OASL Protein Is Mediated by Enhancing Signaling of the RIG-I RNA Sensor. Immunity. 2014; 40: 936–948. https://doi.org/10.1016/j.immuni.2014.05.007 PMID: 24931123

76. Ghosh A, Sarkar SN, Guo W, Bandyopadhyay S, Sen GC. Enzymatic activity of 2'-5'-oligoadenylate synthetase is impaired by specific mutations that affect oligomerization of the protein. J Biol Chem. 1997; 272: 33220–33226. https://doi.org/10.1074/jbc.272.52.33220 PMID: 9407111

77. Pišlar A, Mitrović A, Sabotič J, Pečar Fonović U, Perišić Nanut M, Jakoš T, et al. The role of cysteine peptidases in coronavirus cell entry and replication: The therapeutic potential of cathepsin inhibitors. Hobman TC, editor. PLOS Pathog. 2020; 16: e1009013. https://doi.org/10.1371/journal.ppat.1009013 PMID: 33137165

78. Li J, Xing X, Sun B, Zhao Y, Wu Z. Metallofullerenol Inhibits Cellular Iron Uptake by Inducing Transferrin Tetramerization. Chem—An Asian J. 2017; 12: 2646–2651. https://doi.org/10.1002/asia.201700910 PMID: 28815927

79. Deng C, Zhang P, Wade Harper J, Elledge SJ, Leder P. Mice Lacking p21 CIP1/WAF1 undergo normal development, but are defective in G1 checkpoint control. Cell. 1995; 82: 675–684. https://doi.org/10.1016/0092-8674(95)90039-x PMID: 7664346

80. Mussil B, Suspène R, Aynaud MM, Gauvrit A, Vartanian JP, Wain-Hobson S. Human APOBEC3A Isoforms Translocate to the Nucleus and Induce DNA Double Strand Breaks Leading to Cell Stress and Death. PLoS One. 2013;8. https://doi.org/10.1371/journal.pone.0073641 PMID: 23977391

81. Gytz H, Hansen MF, Skovbjerg S, Kristensen ACM, Hørlyck S, Jensen MB, et al. Apoptotic properties of the type 1 interferon induced family of human mitochondrial membrane ISG12 proteins. Biol Cell. 2017; 109: 94–112. https://doi.org/10.1111/boc.201600034 PMID: 27673746

82. Lee MG, Han J, Jeong SI, Her NG, Lee JH, Ha TK, et al. XAF1 directs apoptotic switch of p53 signaling through activation of HIPK2 and ZNF313. Proc Natl Acad Sci U S A. 2014; 111: 15532–15537. https://doi.org/10.1073/pnas.1411746111 PMID: 25313037

83. Castelli JAC, Hassel BA, Maran A, Paranjape J, Hewitt JA, Li XL, et al. The role of 2'-5' oligoadenylate-activated ribonuclease L in apoptosis. Cell Death Differ. 1998; 5: 313–320. https://doi.org/10.1038/sj.cdd.4400352 PMID: 10200477

84. Weltner J, Balboa D, Katayama S, Bespalov M, Krjutškov K, Jouhilahti EM, et al. Human pluripotent reprogramming with CRISPR activators. Nat Commun. 2018; 9: 2643. https://doi.org/10.1038/s41467-018-05067-x PMID: 29980666

85. Dai Z, Li R, Hou Y, Li Q, Zhao K, Li T, et al. Inducible CRISPRa screen identifies putative enhancers. J Genet Genomics. 2021; 48: 917–927. https://doi.org/10.1016/j.jgg.2021.06.012 PMID: 34531148

86. Colasante G, Qiu Y, Massimino L, Di Berardino C, Cornford JH, Snowball A, et al. In vivo CRISPRa decreases seizures and rescues cognitive deficits in a rodent model of epilepsy. Brain. 2020;143. https://doi.org/10.1093/brain/awaa045 PMID: 32129831

87. Peng R, Wu L-A, Wang Q, Qi J, Gao GF. Cell entry by SARS-CoV-2. Trends Biochem Sci. 2021; 46: 848–860. https://doi.org/10.1016/j.tibs.2021.06.001 PMID: 34187722

88. Matsuyama S, Nao N, Shirato K, Kawase M, Saito S, Takayama I, et al. Enhanced isolation of SARS-CoV-2 by TMPRSS2- expressing cells. Proc Natl Acad Sci U S A. 2020; 117: 7001–7003. https://doi.org/10.1073/pnas.2002589117 PMID: 32165541

89. Biniossek ML, Nägler DK, Becker-Pauly C, Schilling O. Proteomic identification of protease cleavage sites characterizes prime and non-prime specificity of cysteine cathepsins B, L, and S. J Proteome Res. 2011; 10: 5363–5373. https://doi.org/10.1021/pr200621z PMID: 21967108

90. Thornbrough JM, Jha BK, Yount B, Goldstein SA, Li Y, Elliott R, et al. Middle East Respiratory Syndrome Coronavirus NS4b Protein Inhibits Host RNase L Activation. MBio. 2016; 7: e00258. https://doi.org/10.1128/mBio.00258-16 PMID: 27025250

91. Li Y, Banerjee S, Goldstein SA, Dong B, Gaughan C, Rath S, et al. Ribonuclease l mediates the cell-lethal phenotype of double-stranded RNA editing enzyme ADAR1 deficiency in a human cell line. Elife. 2017;6. https://doi.org/10.7554/eLife.25687 PMID: 28362255

92. Li Y, Renner DM, Comar CE, Whelan JN, Reyes HM, Cardenas-Diaz FL, et al. SARS-CoV-2 induces double-stranded rna-mediated innate immune responses in respiratory epithelial-derived cells and cardiomyocytes. Proc Natl Acad Sci U S A. 2021; 118: 1–11. https://doi.org/10.1073/pnas.2022643118 PMID: 33811184

93. Hamano E, Hijikata M, Itoyama S, Quy T, Phi NC, Long HT, et al. Polymorphisms of interferon-inducible genes OAS-1 and MxA associated with SARS in the Vietnamese population. Biochem Biophys Res Commun. 2005; 329: 1234–1239. https://doi.org/10.1016/j.bbrc.2005.02.101 PMID: 15766558

94. He J, Feng D, de Vlas SJ, Wang H, Fontanet A, Zhang P, et al. Association of SARS susceptibility with single nucleic acid polymorphisms of OASI and MxA genes: A case-control study. BMC Infect Dis. 2006;6. https://doi.org/10.1186/1471-2334-6-6 PMID: 16412228

95. Pairo-Castineira E, Clohisey S, Klaric L, Bretherick AD, Rawlik K, Pasko D, et al. Genetic mechanisms of critical illness in COVID-19. Nature. 2021; 591: 92–98. https://doi.org/10.1038/s41586-020-03065-y PMID: 33307546

96. Zhou S, Butler-Laporte G, Nakanishi T, Morrison DR, Afilalo J, Afilalo M, et al. A Neanderthal OAS1 isoform protects individuals of European ancestry against COVID-19 susceptibility and severity. Nat Med. 2021; 27: 659–667. https://doi.org/10.1038/s41591-021-01281-1 PMID: 33633408

97. Kain A Mac, Maarifi G, Aicher S-M, Arhel N, Baidaliuk A, Vallet T, et al. Identification of DAXX As A Restriction Factor Of SARS-CoV-2 Through A CRISPR/Cas9 Screen. bioRxiv. 2021; 58: 2021.05.06.442916. https://doi.org/10.1101/2021.05.06.442916

98. Zang R, Case JB, Yutuc E, Ma X, Shen S, Gomez Castro MF, et al. Cholesterol 25-hydroxylase suppresses SARS-CoV-2 replication by blocking membrane fusion. Proc Natl Acad Sci. 2020; 117: 32105–32113. https://doi.org/10.1073/pnas.2012197117 PMID: 33239446

99. Boehmer DFR, Formisano S, Mueller SA, Kluge M, Metzger P, Rohlfs M, et al. OAS1/RNase L executes 5'-triphosphate RNA-dependent tumor cell apoptosis. Sci Immunol. 2021; 6: eabe2550. https://doi.org/10.1126/sciimmunol.abe2550 PMID: 34272227

100. Walter M, Chen IP, Vallejo-Gracia A, Kim I-J, Bielska O, Lam VL, et al. SIRT5 is a proviral factor that interacts with SARS-CoV-2 Nsp14 protein. bioRxiv. 2022; 2022.01.04.474979. https://doi.org/10.1101/2022.01.04.474979 PMID: 35018374

101. Chen Z, Wang C, Feng X, Nie L, Tang M, Zhang H, et al. Comprehensive analysis of the host-virus interactome of SARS-CoV-2. bioRxiv. 2021; 2020.12.31.424961. https://doi.org/10.1101/2020.12.31.424961

102. Stukalov A, Girault V, Grass V, Karayel O, Bergant V, Urban C, et al. Multilevel proteomics reveals host perturbations by SARS-CoV-2 and SARS-CoV. Nature. 2021; 594: 246–252. https://doi.org/10.1038/s41586-021-03493-4 PMID: 33845483

103. May DG, Martin-Sancho L, Anschau V, Liu S, Chrisopulos RJ, Scott KL, et al. A BioID-derived proximity interactome for SARS-CoV-2 proteins. bioRxiv Prepr Serv Biol. 2021. https://doi.org/10.1101/2021.09.17.460814 PMID: 34580671

104. Samavarchi-Tehrani P, Abdouni H, Knight JDR, Astori A, Samson R, Lin Z-Y, et al. A SARS-CoV-2 – host proximity interactome. bioRxiv. 2020; 2020.09.03.282103. https://doi.org/10.1101/2020.09.03.282103

105. Ren Y, Shu T, Wu D, Mu J, Wang C, Huang M, et al. The ORF3a protein of SARS-CoV-2 induces apoptosis in cells. Cell Mol Immunol. 2020; 17: 881–883. https://doi.org/10.1038/s41423-020-0485-9 PMID: 32555321

106. Li S, Zhang Y, Guan Z, Li H, Ye M, Chen X, et al. SARS-CoV-2 triggers inflammatory responses and cell death through caspase-8 activation. Signal Transduct Target Ther. 2020; 5: 235. https://doi.org/10.1038/s41392-020-00334-0 PMID: 33037188

107. Daniloski Z, Jordan TX, Wessels HH, Hoagland DA, Kasela S, Legut M, et al. Identification of Required Host Factors for SARS-CoV-2 Infection in Human Cells. Cell. 2020; 1–14. https://doi.org/10.1016/j.cell.2020.10.030 PMID: 33147445

108. Wang R, Simoneau CR, Kulsuptrakul J, Bouhaddou M, Travisano KA, Hayashi JM, et al. Genetic Screens Identify Host Factors for SARS-CoV-2 and Common Cold Coronaviruses. Cell. 2021; 184: 106–119.e14. https://doi.org/10.1016/j.cell.2020.12.004 PMID: 33333024

109. Schneider WM, Luna JM, Hoffmann HH, Sánchez-Rivera FJ, Leal AA, Ashbrook AW, et al. Genome-Scale Identification of SARS-CoV-2 and Pan-coronavirus Host Factor Networks. Cell. 2021; 184: 120–132.e14. https://doi.org/10.1016/j.cell.2020.12.006 PMID: 33382968

110. Morsut L, Roybal KT, Xiong X, Gordley RM, Coyle SM, Thomson M, et al. Engineering Customized Cell Sensing and Response Behaviors Using Synthetic Notch Receptors. Cell. 2016; 164: 780–791. https://doi.org/10.1016/j.cell.2016.01.012 PMID: 26830878

111. Livak KJ, Schmittgen TD. Analysis of relative gene expression data using real-time quantitative PCR and the 2-ΔΔCT method. Methods. 2001; 25: 402–408. https://doi.org/10.1006/meth.2001.1262 PMID: 11846609

112. Hill AJ, McFaline-Figueroa JL, Starita LM, Gasperini MJ, Matreyek KA, Packer J, et al. On the design of CRISPR-based single-cell molecular screens. Nat Methods. 2018; 15: 271–274. https://doi.org/10.1038/nmeth.4604 PMID: 29457792

113. Datlinger P, Rendeiro AF, Schmidl C, Krausgruber T, Traxler P, Klughammer J, et al. Pooled CRISPR screening with single-cell transcriptome readout. Nat Methods. 2017; 14: 297–301. https://doi.org/10.1038/nmeth.4177 PMID: 28099430

114. Shalem O, Sanjana NE, Hartenian E, Shi X, Scott DA, Mikkelson T, et al. Genome-scale CRISPR-Cas9 knockout screening in human cells. Science. 2014; 343: 84–87. https://doi.org/10.1126/science.1247005 PMID: 24336571

115. Bateman A, Martin MJ, Orchard S, Magrane M, Agivetova R, Ahmad S, et al. UniProt: The universal protein knowledgebase in 2021. Nucleic Acids Res. 2021; 49: D480–D489. https://doi.org/10.1093/nar/gkaa1100 PMID: 33237286

116. McQuin C, Goodman A, Chernyshev V, Kamentsky L, Cimini BA, Karhohs KW, et al. CellProfiler 3.0: Next-generation image processing for biology. PLoS Biol. 2018; 16: e2005970. https://doi.org/10.1371/journal.pbio.2005970 PMID: 29969450